VOLUME 18 NUMBER 9 SEPTEMBER 2012
www.nature.com/naturemedicine

nature medicine

Evolving HIV therapy
Gene therapy for a ciliopathy
Metabolic control of asymmetric stem cell division

Antiretroviral dynamics determines HIV evolution and predicts therapy outcome

Daniel I S Rosenbloom[1,5], Alison L Hill[1,2,5], S Alireza Rabi[3,5], Robert F Siliciano[3,4] & Martin A Nowak[1]

Despite the high inhibition of viral replication achieved by current anti-HIV drugs, many patients fail treatment, often with emergence of drug-resistant virus. Clinical observations show that the relationship between adherence and likelihood of resistance differs dramatically among drug classes. We developed a mathematical model that explains these observations and predicts treatment outcomes. Our model incorporates drug properties, fitness differences between susceptible and resistant strains, mutations and adherence. We show that antiviral activity falls quickly for drugs with sharp dose-response curves and short half-lives, such as boosted protease inhibitors, limiting the time during which resistance can be selected for. We find that poor adherence to such drugs causes treatment failure via growth of susceptible virus, explaining puzzling clinical observations. Furthermore, our model predicts that certain single-pill combination therapies can prevent resistance regardless of patient adherence. Our approach represents a first step for simulating clinical trials of untested anti-HIV regimens and may help in the selection of new drug regimens for investigation.

The prognosis of HIV infection has dramatically improved since the introduction of highly active antiretroviral therapy (HAART), which, when successful, can bring viral loads below the detection limit, improve immune function and prevent progression to AIDS[1]. Although a complete understanding of how virologic, pharmacologic and host factors interact to determine therapeutic outcome is still lacking, it is clear that a major obstacle to successful treatment is suboptimal drug adherence. Nonadherence can lead to virologic failure and the emergence of drug resistance[2–5].

Because of their high antiviral activity, protease inhibitors are crucial in HIV-1 treatment and are used in three of the five recommended initial regimens and many salvage regimens[6]. Clinical trials have shown that for many drug combinations involving protease inhibitors, treatment failure occurs without resistance mutations in the viral gene encoding protease[7–10], though mutations conferring resistance to other drugs in the regimen are often found. It is generally believed that combination therapy works because it is unlikely that multiple mutations conferring resistance to all drugs in the combination will appear in the same viral genome. Thus, failure without protease inhibitor resistance is puzzling, because it seems to contradict this fundamental explanation for the success of HAART. It is commonly believed that protease inhibitors have a higher "barrier to resistance" than other drugs, meaning that clinically significant protease inhibitor resistance requires the accumulation of multiple mutations in the protease gene[11]. Protease inhibitor resistance also typically occurs at a narrower range of adherence levels than resistance to other drug classes[3,12]. Although these concepts are suggestive, no theory has been developed to explain why patients fail protease inhibitor–based regimens without protease inhibitor resistance.

A resistance mutation may exist before treatment in the latent or active viral populations or may arise during treatment[13]. Drug resistance develops clinically if the mutant strain is selected for over the wild-type strain. Selection depends on the fitness costs and benefits of the mutation, as well as on drug levels, which vary with the dosing interval, the drug half-life and the patient's adherence. Here we use a modeling approach to integrate these factors, enabling us to determine when a resistance mutation will be selected and to predict the outcome of therapy with different drugs. Our results explain the unique adherence-resistance relationship for protease inhibitors and show why patients fail protease inhibitor–based therapy without protease inhibitor resistance.

RESULTS

Defining the mutant selection window

Antiretroviral drugs reduce viral fitness in a dose-dependent manner (**Fig. 1a**). Viral fitness can be summarized as a single parameter, the basic reproductive ratio R_0, which encompasses all phases of the viral life-cycle[14] (**Supplementary Methods**). The Hill dose-response curve describes the relationship between drug concentration and R_0:

$$R_0(D) = \frac{R_{00}}{1 + \left(\frac{D}{\mathrm{IC}_{50}}\right)^m} \quad (1)$$

Here D is drug concentration, IC_{50} is the concentration at which 50% inhibition occurs, and m is a parameter determining steepness of the curve[15,16]. The numerator R_{00} is baseline fitness in the absence of treatment.

[1]Program for Evolutionary Dynamics, Department of Mathematics, Department of Organismic and Evolutionary Biology, Harvard University, Cambridge, Massachusetts, USA. [2]Biophysics Program and Harvard-MIT Division of Health Sciences and Technology, Harvard University, Cambridge, Massachusetts, USA. [3]Department of Medicine, Johns Hopkins University School of Medicine, Baltimore, Maryland, USA. [4]Howard Hughes Medical Institute, Baltimore, Maryland, USA. [5]These authors contributed equally to this work. Correspondence should be addressed to R.F.S. (rsiliciano@jhmi.edu) or M.A.N. (martin_nowak@harvard.edu).

Received 7 May; accepted 27 June; published online 2 September 2012; doi:10.1038/nm.2892

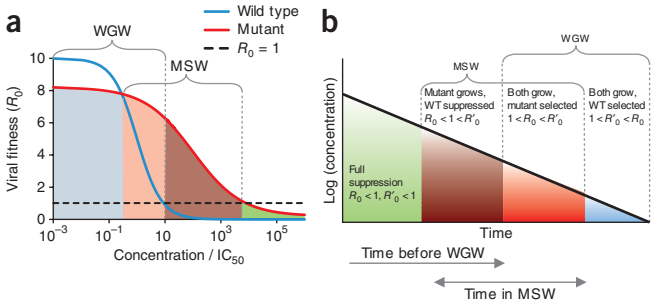

Figure 1 Drug concentrations determine the relative fitness of the wild-type virus and a resistant mutant. (**a**) The fitness of the wild-type virus (R_0, blue line) decreases with increasing drug concentration (here shown normalized by wild-type IC_{50}), following equation (1). A drug-resistant strain (R'_0, red line) is less fit than the wild type at low concentrations but more fit at higher concentrations, owing to an increased IC_{50} or a reduced slope. The MSW is the range of concentrations where a resistant mutant, if present, will grow faster than the wild type and still has $R'_0 > 1$. The WGW is the range of low concentrations where the wild type has $R_0 > 1$, leading to treatment failure without the need for resistance. For drug concentrations in the overlapping range of these windows, virologic failure can occur even without resistance but will be hastened by the appearance of a faster-growing mutant. (**b**) As drug concentrations decay after the last dose is taken, the viral fitness passes through four different selection ranges. Depending on the drug, dose level and mutation, not all of these ranges may exist. The time spent in each selection window is also determined by the drug half-life. WT, wild type.

A drug-resistant mutant is any viral variant that is less inhibited than the wild type for some drug concentration, described by the altered dose-response curve that determines R'_0, the basic reproductive ratio of the resistant virus:

$$R'_0(D) = \frac{R_{00}(1-s)}{1+\left(\frac{D}{\rho IC_{50}}\right)^{m(1+\sigma)}} \quad (2)$$

Mutations have a fitness cost, meaning that the drug-free fitness of the mutant virus is reduced by a fraction s ($0 < s < 1$). In the presence of the drug, the mutation confers a benefit, multiplying the IC_{50} by a factor ρ (the fold change in IC_{50}, $\rho > 1$). Many mutations also reduce the slope (m) of the dose-response curve by a fraction $\sigma < 0$ (ref. 17).

Virologic failure occurs when treatment fails to prevent the growth of virus to high levels. A viral strain grows when $R_0 > 1$. The strain with highest R_0 outcompetes others[14]. The range of drug concentrations where a resistant mutant can cause virologic failure is called the mutant selection window (MSW)[18,19]. Above the MSW, even replication of the mutant is suppressed ($R'_0(D) < 1$), although toxicity may prevent these drug concentrations from being achieved clinically. We here define the wild-type growth window (WGW), where drug concentrations are so low that wild-type virus is not adequately suppressed and failure can occur even without resistance ($R_0(D) > 1$).

The MSW explains therapy outcome patterns

To predict how well each drug suppresses growth of resistant and susceptible strains, we computed the time during a treatment interruption that a patient spends in the MSW and WGW. During treatment interruption, both R_0 and R'_0 increase. Up to four selection ranges can be identified (**Fig. 1b**). Using pharmacokinetic and pharmacodynamic data[16,17] (**Supplementary Table 1**), we determined the time spent in these ranges for 66 drug-mutation pairs (**Fig. 2a**) on the basis of their specific dose-response curves (**Fig. 2b–e**).

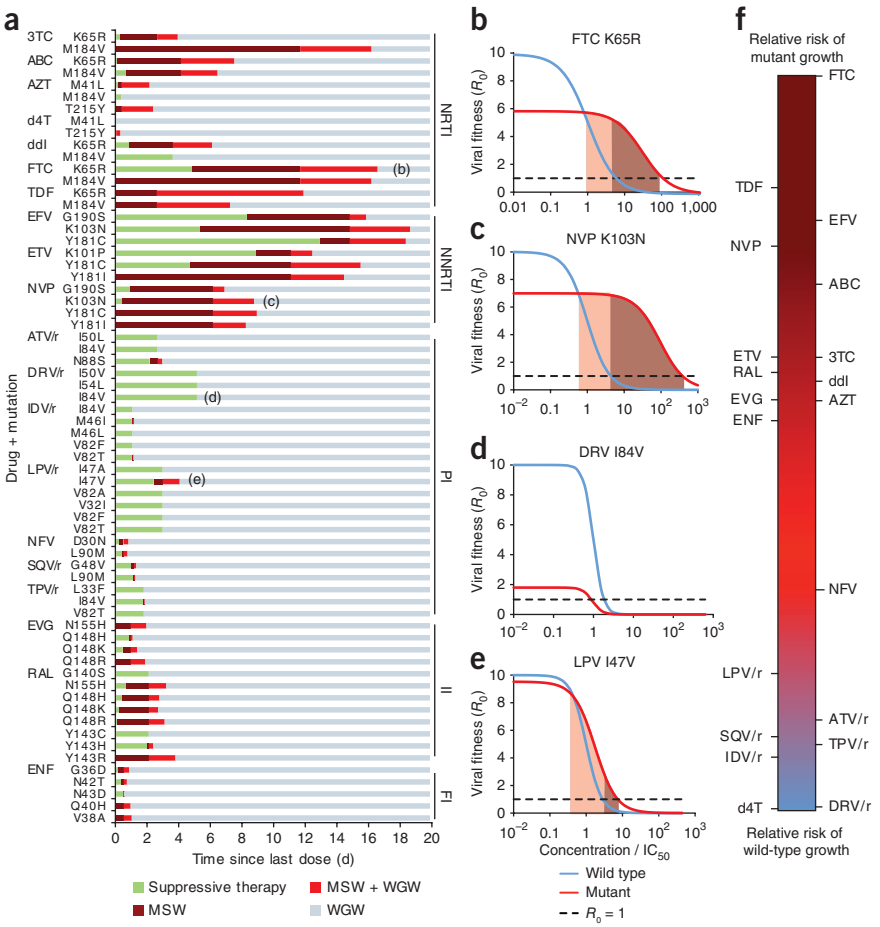

Figure 2 Selection windows can be calculated for particular drug-mutation pairs. (**a**) The distance to the right along each horizontal bar is the time since the last dose, and the color corresponds to the selection window during that time interval (described in **Fig. 1b**). (**b–e**) Examples of dose-response curves (showing drug concentration normalized by wild-type IC_{50}) for drug-mutation combinations indicated in **a**. Shading indicates the MSW. If the cost of a mutation is too high or its benefit (ρ or σ) too low, it is possible that the MSW does not exist. (**f**) Rank of each drug for relative risk of wild-type versus mutant virus growth, independent of the overall risk of therapy failure. For each drug, we show a 'synthetic', worst-case, single-nucleotide mutation (**Supplementary Methods** and **Supplementary Fig. 12**). PI, protease inhibitors; FI, fusion inhibitors; II, integrase inhibitors; ABC, abacavir; FTC, emtricitabine; ATV, atazanavir; TPV, tipranavir; EVG, elvitegravir. Protease inhibitors are often boosted (co-formulated) with ritonovir (/r), which interferes with breakdown in the liver and increases half-life.

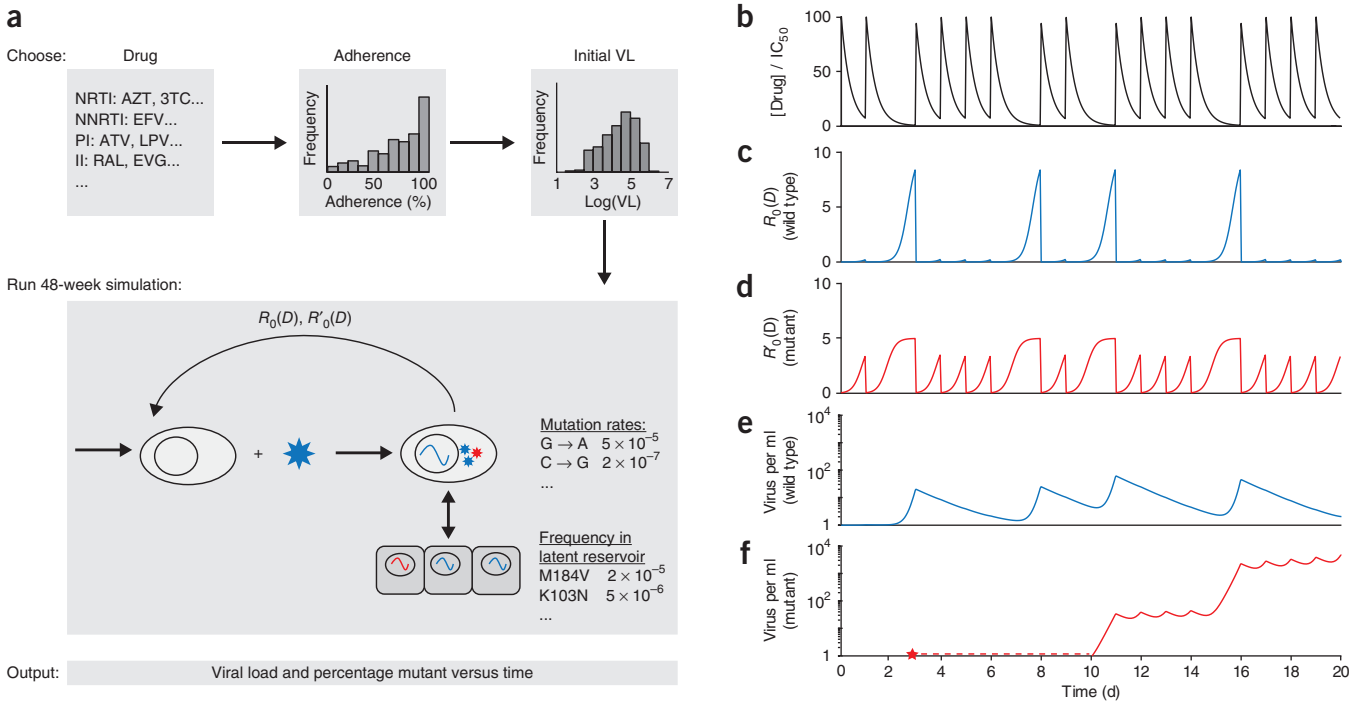

Figure 3 Schematic of algorithm for simulating viral dynamics in a patient undergoing treatment. (**a**) A single simulated patient takes a particular drug (or drug combination) with a designated adherence level, starting with an initial viral load (VL). Over a 48-week clinical trial, drug levels fluctuate and viral load levels are simulated according to a viral dynamics model. (**b**) Drug levels fluctuate according to patient's dosing pattern and pharmacokinetics (dose size, half-life, bioavailability); gaps show missed doses (figure shows single drug). (**c**) Wild-type viral fitness (R_0) fluctuates in response to drug concentration depending on the dose-response curve. (**d**) Fitness of drug-resistant strain (R'_0) depends on an altered dose-response curve; at high drug concentrations, mutant fitness exceeds that of the wild type. (**e**) Wild-type viral load depends on viral dynamics equations, which account for active replication, exit from the latent reservoir and competition between strains. (**f**) A mutant virus may appear (red star) but be below the threshold for detection (dotted red line) before eventually leading to virologic failure. Throughout the figure, blue coloring refers to wild-type virus and red coloring to mutant virus.

For each pair, we determined how soon after the most recent dose the mutant or wild-type virus starts to grow. This quantity is shorter than the expected time until virologic failure, which requires plasma HIV RNA to reach detectable levels and may also depend on the time until mutant virus appears. We examined here only single-point mutations that are fully characterized by their effect on the dose-response curve (equation (2), **Supplementary Tables 2** and **3**). For this reason, we caution that our results may be overly optimistic, as viruses with multiple resistance mutations often appear during infection. The use of our results for clinical recommendations is therefore premature. Extension of this model to multiple mutations is discussed below.

Successful treatment must both minimize the time spent in the MSW and delay entry into the WGW. These two goals are in tension, as shortening the time spent in the MSW (for example, by decreasing drug half-life) can also hasten entry into the WGW (**Fig. 1b**). Results from our model (**Fig. 2a**) suggest that non-nucleoside reverse-transcriptase inhibitors (NNRTIs) are protected against failure via wild-type virus due to their long half-lives but are vulnerable to mutation due to the time spent in the MSW. Protease inhibitors are at the opposite end of the spectrum, with little time spent in the MSW but rapid entry into the WGW. This behavior is caused by high slope parameters (extreme sensitivity to changes in concentration) and short half-lives. These results explain the unique trade-off presented by protease inhibitor therapy: greater protection against the evolution of resistance but vulnerability to wild-type–based virologic failure after short treatment interruptions. This feature is depicted schematically by plotting the drugs along a single axis, which measures the relative risk of mutant growth versus wild-type growth, independent of the overall risk of virologic failure (**Fig. 2f** and **Supplementary Methods**).

Simulation of clinical outcomes

Whereas the MSW and WGW concepts describe instantaneous growth of mutant and wild-type virus for a given drug concentration, virologic failure depends on sustained growth and, therefore, drug concentrations over time. To explain clinical observations across drug classes and adherence levels, we developed a stochastic model of viral evolution (**Fig. 3** and Methods). Our model builds on the large body of previous work modeling HIV therapy[14,20–23] by integrating new data on class-specific drug properties[16] and realistic costs and benefits of mutations[17]. We also modified past approaches by allowing drug concentrations, and hence R_0, to fluctuate, rather than taking time-averages.

We first simulated 48-week trials of single agents in a cohort of patients. The results are presented in two ways: as outcome versus patient adherence at the trial endpoint (**Fig. 4a**) and as outcome versus time for a distribution of patient adherence levels (**Fig. 4b**,**c**).

Consistent with a previous meta-analysis of combination therapy clinical trials[24], our model predicts that the level of adherence necessary for mutant virologic failure differs by drug class (**Fig. 5**). Specifically, for the NNRTIs efavirenz (EFV) and etravirine (ETV), the risk of mutant virologic failure is greatest at low adherence levels; for unboosted protease inhibitors, the risk peaks at a higher adherence level and remains substantial up to 100% adherence; for

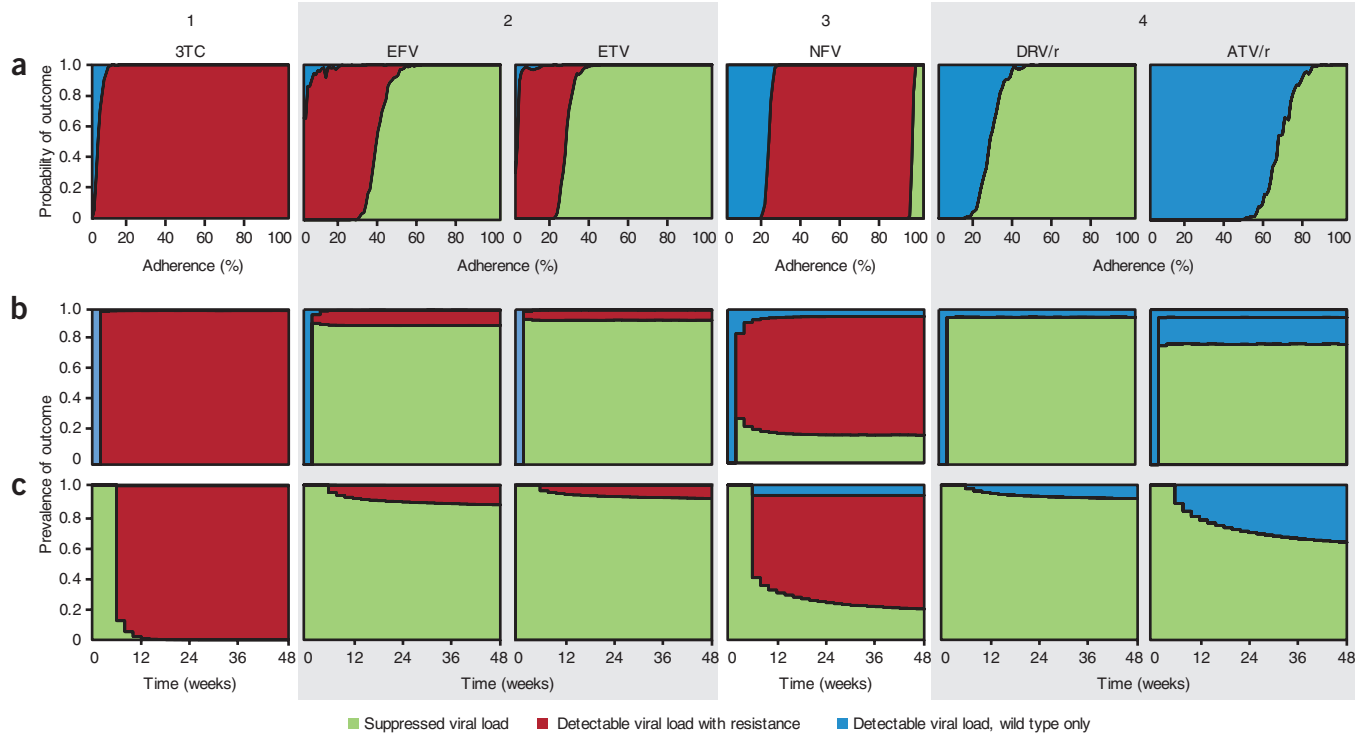

Figure 4 Outcomes for simulated patients in a clinical trial. (**a**–**c**) The height of the area shaded indicates probability of the corresponding outcome at a given adherence level (**a**) or time point (**b**,**c**). (**a**) Adherence is defined as the fraction of scheduled doses taken. These are maintenance trials (see Online Methods). (**b**,**c**) Measurements are taken every 2 weeks for simulated patients with a distribution of adherence levels (**Supplementary Methods** and **Supplementary Fig. 13b**). (**b**) Suppression trials (see Online Methods). (**c**) Maintenance trials. (1) 3TC therapy (pattern includes AZT, ABC, d4T, ENF, EVG, FTC, NVP, RAL, TDF). (2) EFV and ETV therapy. (3) NFV therapy (pattern includes ddI). (4) DRV/r and ATV/r therapy (pattern includes ATV, TPV/r; variation on this pattern described in the Results includes LPV/r, SQV, SQV/r IDV, IDV/r).

boosted protease inhibitors (paired with ritonavir to increase half-life), resistance occurs infrequently and at intermediate adherence levels. Researchers have previously argued that drug half-life and fitness costs of mutations are key factors explaining these general trends[3,12]. By incorporating these factors as parameters, our model formalizes this argument.

In examining simulations of each drug individually (**Supplementary Figs. 1**–**7**), we found four qualitative patterns of outcome, which correspond closely—but not exactly—to drug class (**Fig. 4**).

For most nucleoside reverse-transcriptase inhibitors (NRTIs), the integrase inhibitors, the fusion inhibitor enfuvirtide (ENF) and the NNRTI nevirapine (NVP), even perfect adherence led to mutant virologic failure in all simulated patients. As adherence declined, some wild-type virologic failure occurred. Virologic failure and resistance occurred soon after the trials started. These results are consistent with the notion that monotherapy often leads to rapid evolution of resistance.

For most protease inhibitors and the NNRTIs EFV and ETV, however, perfect adherence resulted in treatment success in simulations. Control of viral replication has been observed in a substantial fraction of patients in protease inhibitor monotherapy trials[25], but similar trials with EFV and ETV have not been carried out. In simulations, declining adherence affected performance of these two drug classes differently.

For the NNRTIs EFV and ETV, there was a large range of low-to-intermediate adherence for which mutant virologic failure was likely. Below this range, wild-type virologic failure became increasingly likely, whereas above this range therapy in the simulated patients succeeded. The size of this range is explained by the low fitness costs of

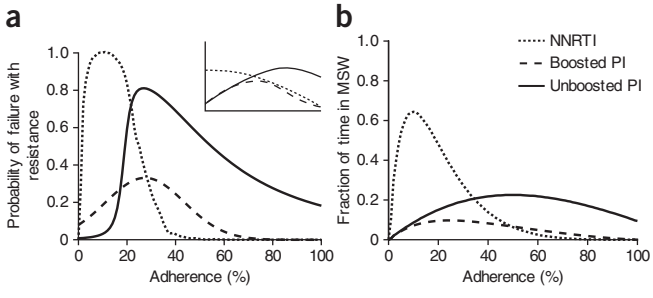

Figure 5 Our calculated adherence-resistance relations are in agreement with those observed in clinical trials. (**a**) Adherence versus simulated probability of resistance in a 48-week suppression trial for a protease inhibitor, a boosted protease inhibitor and an NNRTI. The inset shows a qualitative summary of results from a meta-analysis of clinical trials[24], which agrees with our simulations. (**b**) Adherence versus fraction of time spent in the MSW for the same drugs. Adherence-resistance trends demonstrate that time in MSW is a good proxy for the risk of mutant-based virologic failure. For both plots, curves were generated by averaging over all boosted protease inhibitors, all unboosted protease inhibitors, and the NNRTIs EFV and ETV. Protease inhibitor curves in **a** were fitted to skewed-T distributions to smooth step-like behavior. NVP, which was excluded from this figure, shows a different pattern from the other two NNRTIs; specifically, mutant virologic failure can occur even for perfect adherence (**Supplementary Figs. 1** and **2**).

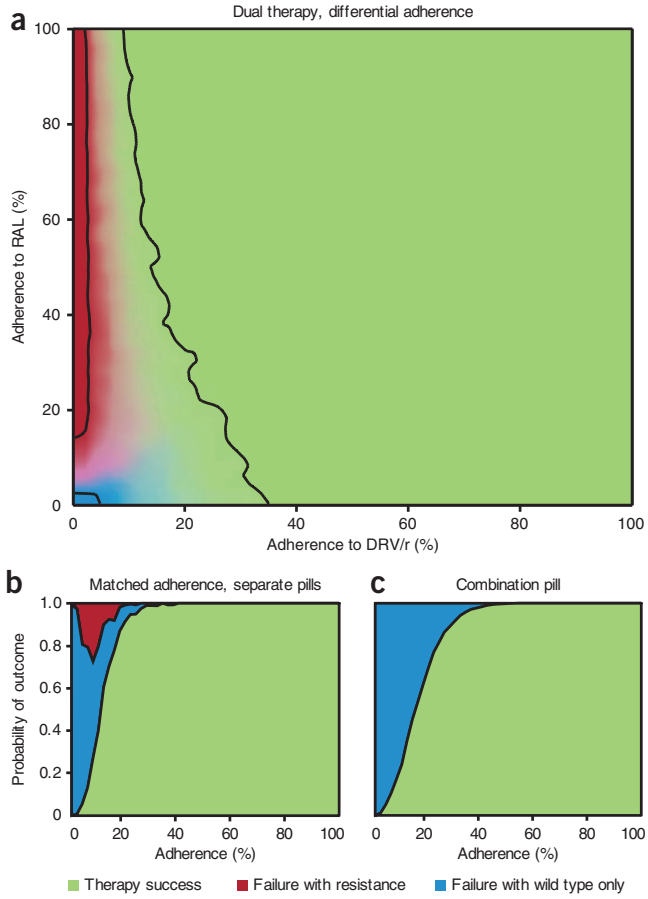

Figure 6 Outcomes of DRV/r plus RAL dual suppression therapy simulations, considering resistant mutants for both drugs. (**a**) Each drug is taken independently, and adherence may differ between them. The brightness of each color at a particular point indicates the probability of the corresponding outcome, with the black contours showing where each outcome occurs 95% of the time. Success depends largely on adherence to DRV/r (success is almost certain if adherence is >50%), whereas the type of failure is determined by adherence to RAL (resistance is almost certain if adherence is >30%). All failure via resistance is due to RAL mutant–based virologic failure. DRV mutant–based virologic failure (virologic failure) never occurs in the simulations. (**b**,**c**) Drugs are taken with equal average adherence. The height of the area shaded indicates probability of the corresponding outcome at that adherence level. (**b**) Drugs are taken as separate pills. Average adherence is the same, but pills are taken independently. (**c**) Drugs are packaged as a combination pill and are always taken together. Mutant virologic failure occurs only when the two drugs are given in separate pills; combination pills eliminate mutant virologic failure but increase the adherence required for near-certain success.

drug-resistant mutations and long half-lives of NNRTIs, which allowed the patient to remain within the MSW for a substantial duration (suggested in ref. 26).

The protease inhibitor nelfinavir (NFV) and the NRTI didanosine (ddI) showed a large range of intermediate adherence leading to mutant virologic failure. Near-perfect adherence was required for treatment success. Under most clinical settings (adherence <95%), our model predicts that these drugs perform similarly to monotherapy with other NRTIs, typically leading to mutant virologic failure.

For many protease inhibitors, a decline from perfect adherence led abruptly from success to wild-type virologic failure, with little or no intermediate range for mutant virologic failure. This result explains the outcomes of clinical studies, which have shown that virologic failure in many boosted protease inhibitor–based regimens (including monotherapy) does not require the evolution of resistance[7–9]. Variations on this pattern exist for some protease inhibitors: simulations of lopinavir (LPV/r), saquinavir (SQV, SQV/r), and indinavir (IDV, IDV/r) showed mutant virologic failure at low and moderate adherence levels, mainly for trials where the initial viral load was high. Still, like all the protease inhibitors simulated except NFV, as adherence declined from the successful range, the first failing outcome observed was wild-type virologic failure (**Supplementary Figs. 1** and **2**).

We also examined the sensitivity of our results to changes in the baseline viral fitness, R_{00} (**Supplementary Figs. 8** and **9**). As the intracellular half-lives of several NRTIs are not definitively established, we tested a range of half-lives for lamivudine (3TC), azidothymidine (AZT), stavudine (d4T), ddI and tenofovir disoproxil fumarate (TDF) (**Supplementary Fig. 10**). Against a strain with higher R_{00}, higher adherence levels were required for treatment success, and there was a wider range of adherence levels for which mutant virologic failure occurred. The effect of increasing half-life was drug dependent, but for most NRTIs simulated, it increased the likelihood of mutant virologic failure.

Explaining outcomes of combination therapy

Equipped with a model of drug interaction, we were able to extend the simulations to combination therapy (**Supplementary Methods** and **Supplementary Fig. 11**). For proof of concept, we use a two-drug combination of the boosted protease inhibitor darunavir (DRV/r) with the integrase inhibitor raltegravir (RAL). The combined effect of these two drugs is given by a Bliss-independent[27] interaction pattern[28], which describes drugs acting on different targets, therefore reducing viral replication multiplicatively. In a recent DRV/r-RAL clinical trial[8], patients experiencing virologic failure had their plasma viral population genotyped. Although 17% of patients tested positive for RAL-resistance mutations in the gene encoding integrase, no patients tested positive for DRV resistance in the gene encoding protease[8]. Our simulation is consistent with this study: treatment failure occurred without DRV resistance (**Fig. 6a**).

RAL-resistant mutants were selected for only when the concentration of DRV/r was low and the concentration of RAL was moderate to high (**Supplementary Fig. 11**). This state of "effective monotherapy"[26] can occur if the drugs are administered as separate pills. If, however, dual therapy were administered as a combination pill, then the two concentrations would rise and fall roughly together, reducing the chance that they reach the discordant levels that select for resistance. Simulation of dual therapy as a single combination pill verified this hypothesis. However, this protection from resistance came at a cost: higher adherence was required to prevent wild-type virologic failure. For example, to ensure a 95% chance of success in the simulation, a patient taking separate pills must be 25% adherent to each pill (**Fig. 6b**), but 35% adherent to a combination pill (**Fig. 6c**). We expect this trend to apply to other drug combinations.

DISCUSSION

Recent efforts to quantify pharmacodynamics[16,17,29], combined with insights into patients' drug-taking behavior[30], have enabled us to develop what is to our knowledge the first explanatory model of virologic failure in agreement with clinical trials. All parameters in our model have direct physical interpretations, and their values were taken directly, or derived from, previous literature. The model was not

fit or trained to match clinical data. Despite our model's simplicity, it can explain the clinically observed drug-class–specific relationship between adherence and outcome[24] (**Fig. 5**). Even without full viral dynamic simulations, a straightforward analysis of the mutant selection window can explain why certain drugs are more likely to select for resistance (**Figs. 2f** and **5b**).

In addition, we address a long-standing mystery of antiretroviral therapy. Even when failure of protease inhibitor–based regimens is documented, mutations that confer resistance to the protease inhibitor appear infrequently[7–10]. Although it is possible that mutations may occur outside the protease-encoding gene[31–34] and escape routine detection, our model provides a more straightforward explanation: due to the sharp slope of protease inhibitor dose-response curves[16], even relatively strong protease inhibitor resistance mutations are selected only in a narrow range of drug concentrations. Moreover, as protease inhibitor concentrations decay rapidly compared to other drugs, they traverse this narrow range quickly, leaving little time for a resistant strain to grow before wild-type–based virologic failure. We predict that patients who fail protease inhibitor therapy with wild-type virus should be able to re-suppress the virus if the same drug is taken with improved adherence. A previous study[12] observed this outcome in patients who failed LPV/r without detectable resistance. Even with protease inhibitors that are more susceptible to resistance, only wild-type virus is detectable when adherence dips below the level guaranteeing success, providing an antiresistance 'buffer' that may warn clinicians of resistance risk. NFV is the sole exception to this pattern, owing to its having the lowest slope and second-highest IC_{50} of the protease inhibitors and consistent with its documented vulnerability to resistance[12].

The tradeoff between protection from resistant and susceptible strains occurs not only between drug classes but also between different formulations of the same drugs. We predict that a new combination pill containing DRV/r and RAL would not lead to resistance, even though the current separate-pill formulation does. This result suggests that some combination pills may be 'resistance proof', but their known benefit of increasing patient adherence must be weighed against the fact that they require higher adherence to prevent wild-type–based virologic failure. This trade-off results from the possibility that a patient who is prescribed multiple pills may at times take only some of them[35], providing partial protection from the virus but allowing entry into a 'zone of monotherapy'[26] that can select for resistance.

We can extend our model to a broader range of combination therapies once interactions between drugs[28] are characterized; these interactions affect the evolution of resistance[36]. Our monotherapy results are a first step for examining how pharmacokinetics and pharmacodynamics determine treatment outcomes. These results can inform innovations in lower-cost maintenance therapy among highly adherent patients, for whom monotherapy shows promise but also poses resistance risks[25]. Specifically, on the basis of our simulations, we propose that EFV and ETV monotherapy may be promising avenues for further study, despite the disheartening performance of monotherapy with the first approved NNRTI, NVP[37], and the ambiguous performance of ETV-based HAART for patients with resistance to the NRTI backbone[38].

Simulations that start with a high viral load (suppression phase) and simulations that start with an undetectable viral load (maintenance phase) generally showed similar outcomes; however, for several drugs, failure with resistance was more likely during the suppression phase. Such differences are often attributed to the presence of preexisting mutants when viral load is high[39–42]. However, in our model, frequent reactivation from the latent reservoir provides a sufficient source of mutants during both phases (**Supplementary Tables 4** and **5**), and ongoing replication is an additional common cause of resistance (**Supplementary Figs. 6** and **7**). The key difference between the two phases is in how virologic failure is defined. As patients remained in suppression simulations until the predefined endpoint, wild-type growth sometimes preceded (and contributed to) growth of the mutant. More frequent measurement of viral load in maintenance simulations improved the chance that virologic failure was diagnosed before resistance reached detectable levels, consistent with clinical meta-analysis[43]. Also consistent with clinical observations[44], continuation of maintenance trials after rebound allowed the possibility of re-suppression, but it sometimes led to emergence of resistance (**Supplementary Fig. 5**).

It is difficult to quantitatively compare our simulations to clinical trials, as adherence is rarely precisely known. We suspect that our results are biased toward success for several reasons. First, we considered only single-point mutations, but strains with multiple mutations may lead to failure at higher adherence levels. Second, we considered neither correlations between consecutive missed doses nor variations in the time of day when a dose is taken, both factors that lead to longer treatment interruptions and increase the chance of virologic failure[20,45–48]. Third, as is common in models of viral dynamics, we assumed that the virus population is homogeneous and well mixed. Actual infections may include subpopulations that grow faster (higher R_0, for example, owing to cell-to-cell transmission[49]) or that reside in tissues that drugs do not fully penetrate[50–52]. For example, the concentration of EFV in the cerebrospinal fluid is only 0.5% of plasma concentrations[53]. As our predictions rely on plasma drug concentrations, they may be optimistic in the case of EFV (see ref. 54 for further discussion). In the absence of strong evidence for these effects, suboptimal adherence is the most likely cause of treatment failure. Given the above limitations, our modeling results should not be taken as clinical recommendations at this stage.

Patients experiencing virologic failure may not respond to a similar regimen in the future[45,55,56], but the precise reasons for this are not clear. The simplest explanation is that growth of a resistant strain during prior treatment makes it more likely this strain will exist in the future[57]. This explanation assumes that, in the absence of prior growth, most resistant mutants are relatively rare. If the diversity (effective population size) of the latent reservoir is not severely depleted over time, then our calculations contradict this assumption for single mutations: even in the absence of prior treatment, a majority of mutations exit the reservoir every few weeks. Resistance is then available to be selected regardless of prior growth. The occurrence of multiple mutations within the same viral genome is unlikely, however, without prior growth. To explain generally how prior virologic failure undermines future treatment, we need to model the long-term accumulation of multistep mutations in the viral population[58,59]. To build such models, it will be important to understand interactions between mutations (including compensatory mutations[54]) and account for recombination[60].

We have emphasized here the variable nature of anti-HIV drug resistance. Common practice classifies a genotype as resistant if it is associated with virologic failure in a meta-analysis of clinical outcomes; otherwise it is sensitive. This categorization is misleading: a mutation's ability to promote viral growth depends on all of the drugs in a regimen, adherence and the other mutations present. As standards of care evolve and study populations change, a mutation may gain or lose resistant status as a result of shifts in these confounding variables.

Our model provides a rigorous alternative for evaluating resistance, by using mechanistic parameters to predict clinical outcomes. Our framework can help researchers prioritize drugs for clinical trials and select regimens for personalized HIV treatment.

METHODS

Methods and any associated references are available in the online version of the paper.

Note: Supplementary information is available in the online version of the paper.

ACKNOWLEDGMENTS

We thank T. Antal, I. Božić, F. Fu, M. Sampah and L. Shen for discussion during the conception of this work, and we thank J. Gallant, J.-B. Michel and P. Pennings for their comments on the manuscript. We thank D. Bangsberg of Massachusetts General Hospital for supplying adherence data from the REACH study (supported by US National Institutes of Health grant R01 MH054907). Simulations were run on the Odyssey cluster supported by the Research Computing Group of Harvard University. We are grateful for support from the US National Institutes of Health (R01 AI081600 (R.F.S., S.A.R.), R01 GM078986 (M.A.N., A.L.H.)), the Bill & Melinda Gates Foundation (M.A.N., A.L.H.), a Cancer Research Institute Fellowship (S.A.R.), a US National Science Foundation Graduate Research Fellowship (D.I.S.R.), the Howard Hughes Medical Institute (R.F.S., S.A.R.), a Canadian Natural Sciences and Engineering Research Council Post-Graduate Scholarship (A.L.H.), the John Templeton Foundation (M.A.N.) and J. Epstein (M.A.N.).

AUTHOR CONTRIBUTIONS

D.I.S.R., A.L.H. and S.A.R. designed the models and conducted the simulations. D.I.S.R., A.L.H., S.A.R., R.F.S. and M.A.N. conceived of the study and wrote the manuscript.

COMPETING FINANCIAL INTERESTS

The authors declare no competing financial interests.

Published online at http://www.nature.com/doifinder/10.1038/nm.2892.
Reprints and permissions information is available online at http://www.nature.com/reprints/index.html.

1. Palella, F.J. *et al.* Declining morbidity and mortality among patients with advanced human immunodeficiency virus infection. HIV Outpatient Study Investigators. *N. Engl. J. Med.* **338**, 853–860 (1998).
2. Vanhove, G.F., Schapiro, J.M., Winters, M.A., Merigan, T.C. & Blaschke, T.F. Patient compliance and drug failure in protease inhibitor monotherapy. *J. Am. Med. Assoc.* **276**, 1955–1956 (1996).
3. Gardner, E.M., Burman, W.J., Steiner, J.F., Anderson, P.L. & Bangsberg, D.R. Antiretroviral medication adherence and the development of class-specific antiretroviral resistance. *AIDS* **23**, 1035–1046 (2009).
4. Maggiolo, F. *et al.* Effect of adherence to HAART on virologic outcome and on the selection of resistance-conferring mutations in NNRTI- or PI-treated patients. *HIV Clin. Trials* **8**, 282–292 (2007).
5. Harrigan, P.R. *et al.* Predictors of HIV drug-resistance mutations in a large antiretroviral- naive cohort initiating triple antiretroviral therapy. *J. Infect. Dis.* **191**, 339–347 (2005).
6. US Department of Health and Human Services Panel on Antiretroviral Guidelines for Adults & Adolescents. Guidelines for the use of antiretroviral agents in HIV-1-infected adults and adolescents. <http://aidsinfo.nih.gov/contentfiles/AdultandAdolescentGL.pdf> (2011).
7. Arribas, J.R. *et al.* The MONET trial: darunavir/ritonavir with or without nucleoside analogues, for patients with HIV RNA below 50 copies/ml. *AIDS* **24**, 223–230 (2010).
8. Taiwo, B. *et al.* Efficacy of a nucleoside-sparing regimen of darunavir/ritonavir plus raltegravir in treatment-naive HIV-1-infected patients (ACTG a5262). *AIDS* **25**, 2113–2122 (2011).
9. Havlir, D.V. *et al.* Drug susceptibility in HIV infection after viral rebound in patients receiving indinavir-containing regimens. *J. Am. Med. Assoc.* **283**, 229–234 (2000).
10. Pulido, F., Arribas, J., Hill, A. & Moecklinghoff, C. No evidence for evolution of genotypic resistance after three years of treatment with darunavir/ritonavir, with or without nucleoside analogues. *AIDS Res. Hum. Retroviruses* published online, doi:10.1089/aid.2011.0256 (20 April 2012).
11. Condra, J.H. Resistance to HIV protease inhibitors. *Haemophilia* **4**, 610–615 (1998).
12. Kempf, D.J. *et al.* Incidence of resistance in a double-blind study comparing lopinavir/ritonavir plus stavudine and lamivudine to nelfinavir plus stavudine and lamivudine. *J. Infect. Dis.* **189**, 51–60 (2004).
13. Noë, A., Plum, J. & Verhofstede, C. The latent HIV-1 reservoir in patients undergoing HAART: an archive of pre-HAART drug resistance. *J. Antimicrob. Chemother.* **55**, 410–412 (2005).
14. Nowak, M.A. & May, R.M.C. *Virus Dynamics: Mathematical Principles of Immunology and Virology* (Oxford University Press, USA, 2000).
15. Chou, T.-C. Derivation and properties of Michaelis-Menten type and Hill type equations for reference ligands. *J. Theor. Biol.* **59**, 253–276 (1976).
16. Shen, L. *et al.* Dose-response curve slope sets class-specific limits on inhibitory potential of anti-HIV drugs. *Nat. Med.* **14**, 762–766 (2008).
17. Sampah, M.E.S., Shen, L., Jilek, B.L. & Siliciano, R.F. Dose-response curve slope is a missing dimension in the analysis of HIV-1 drug resistance. *Proc. Natl. Acad. Sci. USA* **108**, 7613–7618 (2011).
18. Drlica, K. The mutant selection window and antimicrobial resistance. *J. Antimicrob. Chemother.* **52**, 11–17 (2003).
19. Drlica, K. & Zhao, X. Mutant selection window hypothesis updated. *Clin. Infect. Dis.* **44**, 681–688 (2007).
20. Wahl, L.M. & Nowak, M.A. Adherence and drug resistance: predictions for therapy outcome. *Proc. Bio. Sci.* **267**, 835–843 (2000).
21. Wu, H. *et al.* Modeling long-term HIV dynamics and antiretroviral response: effects of drug potency, pharmacokinetics, adherence, and drug resistance. *J. Acquir. Immune Defic. Syndr.* **39**, 272–283 (2005).
22. Smith, R.J. Adherence to antiretroviral HIV drugs: how many doses can you miss before resistance emerges? *Proc. Biol. Sci.* **273**, 617–624 (2006).
23. Rong, L., Feng, Z. & Perelson, A.S. Emergence of HIV-1 drug resistance during antiretroviral treatment. *Bull. Math. Biol.* **69**, 2027–2060 (2007).
24. Bangsberg, D.R., Moss, A.R. & Deeks, S.G. Paradoxes of adherence and drug resistance to HIV antiretroviral therapy. *J. Antimicrob. Chemother.* **53**, 696–699 (2004).
25. Pérez-Valero, I. & Arribas, J.R. Protease inhibitor monotherapy. *Curr. Opin. Infect. Dis.* **24**, 7–11 (2011).
26. Bangsberg, D.R., Kroetz, D.L. & Deeks, S.G. Adherence-resistance relationships to combination HIV antiretroviral therapy. *Curr. HIV/AIDS Rep.* **4**, 65–72 (2007).
27. Bliss, C.I. The toxicity of poisons applied jointly. *Ann. Appl. Biol.* **26**, 585–615 (1939).
28. Jilek, B.L. *et al.* A quantitative basis for antiretroviral therapy for HIV-1 infection. *Nat. Med.* **18**, 446–451 (2012).
29. Shen, L. *et al.* A critical subset model provides a conceptual basis for the high antiviral activity of major HIV drugs. *Sci. Transl. Med.* **3**, 91ra63 (2011).
30. Bangsberg, D.R. *et al.* Adherence-resistance relationships for protease and non-nucleoside reverse transcriptase inhibitors explained by virological fitness. *AIDS* **20**, 223–231 (2006).
31. Nijhuis, M. *et al.* A novel substrate-based HIV-1 protease inhibitor drug resistance mechanism. *PLoS Med.* **4**, e36 (2007).
32. Parry, C.M. *et al.* Gag determinants of fitness and drug susceptibility in protease inhibitor–resistant human immunodeficiency virus type 1. *J. Virol.* **83**, 9094–9101 (2009).
33. Dam, E. *et al.* Gag mutations strongly contribute to HIV-1 resistance to protease inhibitors in highly drug-experienced patients besides compensating for fitness loss. *PLoS Pathog.* **5**, e1000345 (2009).
34. Gupta, R.K. *et al.* Full length HIV-1 gag determines protease inhibitor susceptibility within *in vitro* assays. *AIDS* **24**, 1651–1655 (2010).
35. Gardner, E.M. *et al.* Differential adherence to combination antiretroviral therapy is associated with virological failure with resistance. *AIDS* **22**, 75–82 (2008).
36. Michel, J.-B., Yeh, P.J., Chait, R., Moellering, R.C. & Kishony, R. Drug interactions modulate the potential for evolution of resistance. *Proc. Natl. Acad. Sci. USA* **105**, 14918–14923 (2008).
37. Cheeseman, S.H. *et al.* Phase I/II evaluation of nevirapine alone and in combination with zidovudine for infection with human immunodeficiency virus. *J. Acquir. Immune Defic. Syndr. Hum. Retrovirol.* **8**, 141–151 (1995).
38. Ruxrungtham, K. *et al.* Impact of reverse transcriptase resistance on the efficacy of TMC125 (etravirine) with two nucleoside reverse transcriptase inhibitors in protease inhibitor-naive, nonnucleoside reverse transcriptase inhibitor-experienced patients: study TMC125–C227. *HIV Med.* **9**, 883–896 (2008).
39. Bonhoeffer, S. & Nowak, M.A. Pre-existence and emergence of drug resistance in HIV-1 infection. *Proc. Biol. Sci.* **264**, 631–637 (1997).
40. Paredes, R. *et al.* Pre-existing minority drug-resistant HIV-1 variants, adherence, and risk of antiretroviral treatment failure. *J. Infect. Dis.* **201**, 662–671 (2010).
41. Jourdain, G. *et al.* Association between detection of HIV-1 DNA resistance mutations by a sensitive assay at initiation of antiretroviral therapy and virologic failure. *Clin. Infect. Dis.* **50**, 1397–1404 (2010).
42. Simen, B.B. *et al.* Low-abundance drug-resistant viral variants in chronically HIV-infected, antiretroviral treatment–naive patients significantly impact treatment outcomes. *J. Infect. Dis.* **199**, 693–701 (2009).
43. Gupta, R.K. *et al.* Virological monitoring and resistance to first-line highly active antiretroviral therapy in adults infected with HIV-1 treated under who guidelines: a systematic review and meta-analysis. *Lancet Infect. Dis.* **9**, 409–417 (2009).
44. Hoffmann, C.J. *et al.* Viremia, resuppression, and time to resistance in human immunodeficiency virus (HIV) subtype c during first-line antiretroviral therapy in South Africa. *Clin. Infect. Dis.* **49**, 1928–1935 (2009).
45. Parienti, J.-J. Not all missed doses are the same: sustained NNRTI treatment interruptions predict HIV rebound at low-to-moderate adherence levels. *PLoS ONE* **3**, e2783 (2008).

46. Parienti, J.-J. Average adherence to boosted protease inhibitor therapy, rather than the pattern of missed doses, as a predictor of HIV RNA replication. *Clin. Infect. Dis.* **50**, 1192–1197 (2010).
47. Liu, H. *et al.* Repeated measures analyses of dose timing of antiretroviral medication and its relationship to HIV virologic outcomes. *Stat. Med.* **26**, 991–1007 (2007).
48. Kastrissios, H. *et al.* Characterizing patterns of drug-taking behavior with a multiple drug regimen in an AIDS clinical trial. *AIDS* **12**, 2295–2303 (1998).
49. Sigal, A. *et al.* Cell-to-cell spread of HIV permits ongoing replication despite antiretroviral therapy. *Nature* **477**, 95–98 (2011).
50. Kepler, T.B. & Perelson, A.S. Drug concentration heterogeneity facilitates the evolution of drug resistance. *Proc. Natl. Acad. Sci. USA* **95**, 11514–11519 (1998).
51. Schnell, G., Price, R.W., Swanstrom, R. & Spudich, S. Compartmentalization and clonal amplification of HIV-1 variants in the cerebrospinal fluid during primary infection. *J. Virol.* **84**, 2395–2407 (2010).
52. van Marle, G. *et al.* Compartmentalization of the gut viral reservoir in HIV-1 infected patients. *Retrovirology* **4**, 87 (2007).
53. Best, B.M. *et al.* Efavirenz concentrations in CSF exceed IC_{50} for wild-type HIV. *J. Antimicrob. Chemother.* **66**, 354–357 (2011).
54. Hill, A.L., Rosenbloom, D.I.S. & Nowak, M.A. Evolutionary dynamics of HIV at multiple spatial and temporal scales. *J. Mol. Med.* **90**, 543–561 (2012).
55. Hirsch, M.S. *et al.* Antiretroviral drug resistance testing in adult HIV-1 infection: recommendations of an International AIDS Society–USA panel. *J. Am. Med. Assoc.* **283**, 2417–2426 (2000).
56. Lima, V.D. *et al.* Differential impact of adherence on long-term treatment response among naive HIV-infected individuals. *AIDS* **22**, 2371–2380 (2008).
57. Boltz, V.F. *et al.* Role of low-frequency HIV-1 variants in failure of nevirapine-containing antiviral therapy in women previously exposed to single-dose nevirapine. *Proc. Natl. Acad. Sci. USA* **108**, 9202–9207 (2011).
58. Nowak, M.A. *et al.* Antigenic diversity thresholds and the development of AIDS. *Science* **254**, 963–969 (1991).
59. Shankarappa, R. *et al.* Consistent viral evolutionary changes associated with the progression of human immunodeficiency virus type 1 infection. *J. Virol.* **73**, 10489–10502 (1999).
60. Neher, R.A. & Leitner, T. Recombination rate and selection strength in HIV intra-patient evolution. *PLoS Comput. Biol.* **6**, e1000660 (2010).

ONLINE METHODS

Pharmacokinetics, pharmacodynamics and the mutant selection window. Viral fitness followed equation (1) with parameters R_{00}, IC_{50} and m. Fitness of resistant mutants followed equation (2) with parameters s, ρ and σ. (**Supplementary Tables 1–3**). Relative wild-type and mutant viral fitness values $R_0(D) / R_{00}$ and $R'_0(D) / R_{00}$ were measured using *in vitro* assays and were fit to Hill curves to determine the parameters IC_{50}, m, σ, ρ and s; these values were reported previously[16,17]. We estimated absolute *in vivo* viral fitness in the absence of drugs (R_{00}) using measurements from previous studies (**Supplementary Methods**). We modeled drug concentration as instantaneously increasing after a dose to the steady-state peak concentration (C_{max}) and then decaying exponentially (with half-life $T_{1/2}$) to the trough concentration (C_{min}) before the subsequent dose. When doses were missed (representing suboptimal adherence), the concentration continued to decay, and a subsequent dose increased the concentration by $\Delta C = C_{max} - C_{min}$.

We determined the bounds of the MSW by solving for D in $R_0(D) = R'_0(D)$ and $R'_0(D) = 1$. We determined the upper bound of the WGW by solving $R_0(D) = 1$. We computed the time after a single dose when a particular concentration D was reached by solving for t in $D = C_{max} \times 2^{-t/T_{1/2}}$.

The MSW concept as applied here to antiretroviral therapy was adapted from the extensive literature on antibiotic resistance. Both *in vitro* and *in vivo*, drug concentrations that fluctuate within the MSW lead to the development of resistance, but those outside it do not (reviewed in ref. 19). Although some studies of antibiotic-resistant *Escherichia coli* have found no upper limit to the MSW[61], no such results are known for antiretroviral resistance. The definition of the MSW most commonly used in antibiotic work is slightly different from the one we use, with the lower limit defined as $R_0(D) = 1$ because of experimental constraints[18]. We have chosen to modify this definition, as selection for the mutant can occur even at lower drug concentrations where $R_0(D) > 1$ (ref. 62). The MSW and WGW can be described for each drug during combination therapy (**Supplementary Methods**).

Simulation of the viral dynamics model. Our model for HIV dynamics during antiretroviral drug treatment uses equations common in the literature[14]. These equations track the number of uninfected $CD4^+$ cells, amount of free virus and number of infected $CD4^+$ cells. A constant number of uninfected cells are produced each day, and they die at a constant rate. Cells are infected at a rate proportional to the number of uninfected cells, the amount of virus, and the viral fitness. Virion production from infected cells is described by the burst rate, and virions are cleared at a constant rate. Infected cells have a higher death rate than uninfected cells. Additionally, we include a population of long-lived infected cells in the latent reservoir, which activate at a constant daily rate regardless of viral fitness. Because we are interested only in viral dynamics during treatment and at the initial stages of failure, we have ignored the effects of the immune response. Viral fitness, and hence the rate of infection of new $CD4^+$ cells, is determined by the baseline R_0 and the drug concentration. All equations and parameters are given in the **Supplementary Methods** and **Supplementary Table 6**. In the **Supplementary Methods**, we also derive a simplified form of HIV dynamics that requires fewer parameters and only one state variable per viral strain; we used this simplified model to design our simulations. More detailed models that explicitly track multiple stages of the viral life cycle may more accurately reflect some short-term dynamics, such as lags in viral growth during acute infection or lags in viral decay during the early days of treatment[63,64]. Summarizing viral fitness by a single parameter (R_0) smoothes out these dynamics.

There may be multiple strains of virus (wild-type and mutants) and consequently multiple types of infected cells. Even in the absence of drug, mutations will arise due to random errors in replication, though they will be selected against due to their fitness cost (s). Each mutation appears at a rate u that depends on the particular nucleotide changes required to effect the desired amino acid substitution (**Supplementary Tables 2**, **3** and **7**). The balance between these two processes results in all mutations being present in the population at an expected low level u / s, called mutation-selection equilibrium[14,65]. We assume that the plasma virus population reaches this equilibrium in each patient before treatment (that is, that sufficient time has passed between initial infection and treatment initiation and that no prior treatment has selected for resistance to the particular drug being studied) and that the population in the latent reservoir is representative of the plasma population (**Supplementary Tables 4** and **5**). *De novo* mutations occur with a probability u during replication.

We used stochastic simulations to study the dynamics of the system described. Many mutations have been characterized for each drug, and to model a realistic worst-case scenario we considered a single synthetic mutant defined as having the highest benefits (ρ, negative σ), lowest cost (s), highest mutation rate and highest equilibrium frequency (due to mutation-selection balance) of all the single-nucleotide mutants known for that drug. Each monotherapy simulation therefore tracked only two strains, wild-type and mutant. For dual therapy, we considered three strains: wild-type, resistant to drug 1, and resistant to drug 2. Simulations modeled 48-week trials, using discrete time-steps of Δt = 30 min. All simulations were done in Matlab R2010b. The full details of the algorithm for simulating a single patient are given in the **Supplementary Methods**.

In maintenance trials, patients began with full viral suppression (2 RNA copies per ml, c ml^{-1}) and underwent monotherapy for 48 weeks or until virologic failure, whichever occurred first. Virologic failure was defined as 'confirmed rebound': two consecutive weekly measurements (starting at week 5) with viral load above 200 c ml^{-1}. In suppression trials, patients began with a realistic distribution of treatment-naive viral loads (between 3,000 and 10^6 c ml^{-1}) (**Supplementary Fig. 13a**) and underwent monotherapy for a full 48 weeks. We tracked measurements every 2 weeks. Virologic failure was defined as a viral load above 50 c ml^{-1} at week 48. In both types of trials, virologic failure was classified as 'with resistance' if at least 20% of the viral population at the time of detection was mutant.

We simulated imperfect adherence by allowing each dose to be missed with a constant probability given by the expected adherence level parameter. In reporting outcomes versus time, we simulated patients with a distribution of adherence levels taken from a study using unannounced pill counts[30]. For simulations with two drugs, the value of adherence may be different for each drug, allowing for 'differential adherence', which has been observed in many studies[35]. Even when adherence to the two drugs has the same average value, the drugs can be simulated as two separate pills (allowing each pill to be taken or forgotten independently) or as a single combination pill (causing the two drug concentrations to rise and fall in lockstep).

61. Zhao, X. & Drlica, K. Restricting the selection of antibiotic-resistant mutant bacteria: measurement and potential use of the mutant selection window. *J. Infect. Dis.* **185**, 561–565 (2002).
62. Gullberg, E. *et al.* Selection of resistant bacteria at very low antibiotic concentrations. *PLoS Pathog.* **7**, e1002158 (2011).
63. Sedaghat, A.R., Dinoso, J.B., Shen, L., Wilke, C.O. & Siliciano, R.F. Decay dynamics of HIV-1 depend on the inhibited stages of the viral life cycle. *Proc. Natl. Acad. Sci. USA* **105**, 4832–4837 (2008).
64. Ribeiro, R.M. *et al.* Estimation of the initial viral growth rate and basic reproductive number during acute HIV-1 infection. *J. Virol.* **84**, 6096–6102 (2010).
65. Ribeiro, R.M., Bonhoeffer, S. & Nowak, M.A. The frequency of resistant mutant virus before antiviral therapy. *AIDS* **12**, 461–465 (1998).

doi:10.1038/nm.2892

Supplementary information

Antiretroviral dynamics determines HIV evolution and predicts therapy outcome

Daniel I. S. Rosenbloom[*,1], Alison L. Hill[*,1,2], S. Alireza Rabi[*,3], Robert F. Siliciano[†3,4], and Martin A. Nowak[†1]

[1]Program for Evolutionary Dynamics, Department of Mathematics, Department of Organismic and Evolutionary Biology, Harvard University, Cambridge, MA 02138, USA
[2]Biophysics Program and Harvard-MIT Division of Health Sciences and Technology, Harvard University, Cambridge, MA 02138 USA
[3]Department of Medicine, Johns Hopkins University School of Medicine, Baltimore, MD 21205, USA
[4]Howard Hughes Medical Institute, Baltimore, MD 21205, USA
[*]Authors contributed equally to work
[†]To whom correspondence should be addressed. Email: rsiliciano@jhmi.edu, martin_nowak@harvard.edu

Contents

List of Tables

List of Figures

1 Supplementary Methods

1.1 Viral dynamics model

The following system of equations models the dynamics of multiple strains ($i = 1, 2, \ldots, n$) of HIV in a patient:

$$\begin{aligned} \dot{x} &= \lambda - \sum_{i=1}^{n} \beta_i x v_i - d_x x \\ \dot{y}_i &= \beta_i x v_i + A_i - d_y y_i \\ \dot{v}_i &= k_i y_i - d_v v_i \end{aligned} \tag{1}$$

where state variables x, y_i, and v_i are the number of infectable $CD4^+$T-cells, the number of actively infected cells of strain i, and the number of free virus particles of strain i, respectively. The number of latently infected cells is considered to be constant, as it doesn't decay significantly over the course of a clinical trial, and so latently infected cells of strain i activate at a constant rate A_i. Active cells produce virus at rate k_i and die at rate d_y, and virus is cleared at rate d_v. The infectivity

parameter β_i determines the rate at which virus of strain i infects susceptible host cells. Host cell dynamics are determined by production rate λ and death rate d_x.

When $A_i = 0$ for a strain i, this model reduces to the traditional viral dynamics model[14]. For that model we can describe the *basic reproductive ratio*, which is defined as the number of new infections generated by a lone infected cell before it dies. Strain i will only have a positive growth rate and be capable of sustaining an infection if its basic reproductive ratio, $R_{0i} := \lambda\beta_i k_i / \left(d_x d_y d_v\right)$, is greater than 1. In the model we present here the latent reservoir provides a constant source of virus (A_i), which removes the threshold criteria for R_0, although this value still describes viral fitness and the amount of ongoing viral replication.

For a single strain, the unique non-negative steady-state solution to our model is

$$y_1 = \frac{\lambda}{2d_y R_{01}}\left[R_{01}\left(\frac{A_1}{\lambda}+1\right) - 1 + \sqrt{R_{01}^2\left(\frac{A_1}{\lambda}+1\right)^2 + 2R_{01}\left(\frac{A_1}{\lambda}-1\right)+1}\right] \tag{2}$$

In our model, for $R_{0i} > 1$, strain i grows to a high steady state that depends on availability of host cells and the abundance of other strains. There are several limiting cases that can be derived from equation (2). In the absence of other strains (or if $R_{0j} \ll 1$ for all $j \neq i$), and for small reactivation $A_i \ll \lambda$, strain i grows to the steady state $y_i \approx \tilde{Y}_i := \lambda\left(R_{0i}-1\right)/\left(d_y R_{0i}\right)$. The value $\tilde{Y}_i$ is the setpoint viral load that is maintained by replication alone, without additional contribution from the latent reservoir. The residual active infection maintained by the latent reservoir in complete absence of viral replication ($R_{0i} = 0$) is $\tilde{y}_{0i} := A_i/d_y$. For positive $R_{0i} < 1$, strain i reaches a low steady state $y_i \approx \tilde{y}_i := \tilde{y}_{0i}/\left(1 - R_{0i}\right)$. Since anti-HIV drugs act by decreasing β_i and k_i, the value of R_{0i} is understood to depend on the current drug concentration(s).

To eliminate some of the model parameters and smooth the high-frequency fluctuations that

may have little clinical impact over the course of a drug trial, we study a simplified version of the model in equation (1). We assume that v_i and x are at equilibrium relative to y_i. This allows us to derive a reduced n-dimensional model:

$$\dot{y}_i = A_i + d_y y_i \left[\frac{\lambda R_{0i}}{\lambda + \sum_{j=1}^{n} R_{0j} d_y y_j} - 1 \right] \tag{3}$$

When the total infection is small, the summation term vanishes, and $\dot{y}_i \approx A_i + d_y y_i (R_{0i} - 1)$. For $R_{0i} \ll 1$, nearly all of strain i is produced by exit from the reservoir; y_i therefore approaches a value near $\tilde{y}_{0i}$. As the total infection grows (assuming $R_{0i} > 1$ for one or more i), the fractional term approaches 1, describing saturation of the limiting resource, at which point new infection events are balanced precisely by death of infected cells and y_i approaches a value near $\tilde{Y}_i$. This reduced model has identical steady state values of virus and $CD4^+$cells as the full model, but smooths out fluctuations in infection size caused by the dynamics of total $CD4^+$cells. Because we focus on initial virologic failure, which occurs at relatively low viral loads, the fluctuations in $CD4^+$cell levels are minor, and the approximation captures the full dynamics (equation (1)) well.

We can account for mutation by including the mutation rate matrix Q, where Q_{ij} describes the probability that an infected cell of type j gives rise to one of type i:

$$\dot{y}_i = A_i + \frac{\lambda d_y \sum_{j=1}^{n} y_j R_{0j} Q_{ij}}{\lambda + \sum_{j=1}^{n} R_{0j} d_y y_j} - d_y y_i \tag{4}$$

1.2 Model parameters

The value of R_{0i} at each point in time depends on the baseline basic reproductive ratio ($R_{00} = 10$, see below), the current drug concentration(s), and parameters describing resistance of the strain, as described by equations 1 and 2 in the main text. The death rate of actively infected cells, d_y, is 1 per day[66]. **Supplementary Table 6** summarizes the parameters used in the model.

1.2.1 Basic reproductive ratio

The basic reproductive ratio (R_0) combines various components of viral fitness into a single number. $R_0 > 1$ is required for the virus to have a positive growth rate and sustain an infection. The baseline R_0, which we denote R_{00}, is defined in the absence of drug and has been estimated in past studies by measuring the increase in viral load during the early days of acute infection or during planned treatment interruption. During the acute phase, before the CTL response develops, typical values for R_{00} are 10-20(ref. 64;67). After this initial phase, R_{00} declines to 2-5, with some outliers as high as 6-11 (ref. 68-72) . Based on these findings, we chose a value of R_{00}=10 to present our results. We also checked sensitivity to this parameter by using larger and smaller R_{00} values (**Supplementary Figures 8 -9**).

We can also double-check that our value of R_{00} from the literature is consistent with an independent set of measurements. The growth rate of a mutant strain in the absence of drug is $R_{00} * (1 - s)$ (see equation 1 in the main text), where s is the reduction in the replication capacity of the mutant virus. If $R_{00} * (1 - s) > 1$, then a mutant strain will expand in the absence of drug. If this condition fails, then the mutant strain would never be detected at high abundance (ignoring secondary or compensatory mutations). Since all the resistance mutations that we study do occur clinically, we expect that $R_{00} > 1/(1 - s)$ should almost always hold. 95% of the mutations studied have $s < 0.9$, for which the positive growth condition is satisfied for the value $R_{00} = 10$.

To maintain consistency with the chosen value $R_{00} = 10$, we capped the cost of mutations used in the viral dynamics simulation at $s = 0.9$, guaranteeing that no mutant's baseline R_0 would be less than 1. Values of s that are negative are also inappropriate for our model, as they imply that the resistant mutant is more fit than the wild type even in the absence of the drug, causing the mutant to be prevalent at baseline. Measurements of s that were close to 0 or negative were assumed to be caused by experimental error, and so we set these values to $s = 0.05$ to represent a small cost to these mutations.

1.2.2 Latent reservoir exit rate

Based on the following argument, we estimate the total reservoir exit rate $\sum_i A_i$ to be 3000 cells per day. The exit rate for a particular mutant strain is determined by multiplying by the equilibrium frequency of pre-existing mutants, u/s. (Our simulation treats each exit as an independent event; use of this modeling approach implicitly assumes that the reservoir was seeded by a large, diverse population, and that its diversity, or effective population size, is maintained over time.) Viral loads of around 2 RNA copies per mL are maintained in patients on maximally suppressive HAART[73]. The rate of exit from the reservoir must be enough to account for this residual viral load, since ongoing replication is negligible. This viral load corresponds to $\approx 3 \times 10^3$ plasma virions (for a 70 kg person with 3L plasma). It has been shown, for a wide range of viral loads, that the total number of infected cells in a patient is roughly equal to the number of plasma virions[74]. The infection size $\sum y_i \approx (\sum A_i)/d_y$ is therefore 3×10^3, implying a total reservoir exit rate of 3000 cells per day.

Alternately, we can estimate the number of infected cells by noting that total viral production (burst from infected cells) must balance total viral clearance (breakdown of free virus in lymphatic tissue). Using parameters previously established[75], free virus in lymph tissues is 100 times as abundant as virus in the extracellular fluid, and so would be about 1.5×10^6 virions (based on

15L ECF) for this example. This paper also determined that the ratio of viral burst size to viral clearance rate is typically 500 virions per cell (e.g., k_i = 10,000 virions per day per cell; d_v = 20 per day). These figures again imply an infection size of 3000 cells.

Our calculations also agree with the results of a model which examined the many years-long decay of the latent reservoir in HAART patients[76]. Although this model used different sources for parameter values, it is consistent with an exit rate of 3000 cells per day, as long as the reservoir is not significantly depleted.

1.2.3 Host cell production rate

For a single wild-type strain in the absence of drug, the model (equation (3)) provides $\lambda = \tilde{Y} d_y R_{00} / (R_{00} - 1)$, where $\tilde{Y}$ is the total number of infected cells at infection setpoint. As established above, this value is approximately equal to the number of plasma virions at setpoint. We considered setpoint viral loads from 3000 to 10^6 RNA copies per ml plasma, or 4.5×10^6 to 1.5×10^9 total plasma virions. These values give a range of 5×10^6 to 1.7×10^9 cells per day for λ.

1.2.4 Resistance mutation rates

The mutation rate matrix entry Q_{ij} describes the probability that strain j reproduces to create strain i. We include only single step mutations from the wild type ($j = 1$) to another strain i (at rate u_i) and ignore back-mutation. Therefore $Q_{i1} = u_i$ for $i > 1$, $Q_{1,1} = 1 - \sum_{k=2}^{n} u_k$, $Q_{ii} = 1$ for $i > 1$ and $Q_{ij} = 0$ for all other entries.

The overall mutation rate for HIV is 3×10^{-5} per base per replication cycle[77], and recent work has shown that the rate varies considerably depending on the specific base changes involved. The nucleotide mutation matrix used in this study was derived by normalizing mutation accumulation data from a study of HIV replication of lacZα reporter sequence[78]. The normalized data was

then rescaled to convert from the lacZα base composition to the HIV consensus sequence base composition[79]. Specifically:

1. Define the variables:

   - $u = 3 \times 10^{-5}$ is the average per-site mutation rate of HIV.
   - s_{xy} is the total number of single-nucleotide substitutions from base x to base y, combining data from both the forward and reverse orientations of lacZα in Table 3A of Abram et al.[78].
   - s_{x*} is the total number of single-nucleotide substitutions from base x to any other base.
   - S is the total number of single-nucleotide substitutions overall.
   - n_x and n'_x are the abundance of base x in the reporter sequence and in the HIV consensus sequence, respectively. N and N' are the lengths of the two sequences, respectively.
     - $n_T = 37, n_C = 56, n_A = 36, n_G = 45; N = 174$
     - $n'_T = 2163, n'_C = 1772, n'_A = 3411, n'_G = 2373; N' = 9719$

2. Calculate the relative mutability of each base x in the reporter sequence, $r_x = (s_{x*}/n_x) \,/\, (S/N)$. A value $r_x > 1$ indicates that base x is more mutable than the average, while $r_x < 1$ indicates the opposite.

3. The per-site mutation rates from all bases x, denoted u_{x*}, are assumed to be proportional to the relative mutabilities r_x. To compute the values u_{x*}, scale the relative mutabilities so that the sum $n'_T u_{T*} + n'_C u_{C*} + n'_A u_{A*} + n'_G u_{G*}$ equals $N'u$, the genomic mutation rate of HIV (about 0.3 substitutions per replication). The correct scaling factor is $u_{x*}/r_x = N'u/\left(\sum r_x n'_x\right)$.

4. To determine the individual rates u_{xy}, partition each value u_{x*} proportional to the substitutions counted in the reported sequence; that is, $u_{xy} = u_{x*}\left(s_{xy}/s_{x*}\right)$.

Supplementary Table 7 gives the resulting per-site probability (u_{xy}) for each nucleotide substitution in a single round of viral replication.

Mutation rates were calculated only for those amino acid substitutions which could be achieved via a single nucleotide change. All drugs studied had at least one such substitution that conferred resistance. For each possible starting codon, the rate of substitution equals the sum of all rates of nucleotide substitutions that achieve the desired amino acid change. The mutation rate u then equals the average of rates for all possible starting codons, weighted by the probability of finding that codon (based on the HIV consensus sequence base composition) (used in **Supplementary Tables 4, 5**).

1.3 Simulation algorithm

We used stochastic simulations to study the dynamics of the system described in equation (3) with mutation. Multiple mutations have been characterized for each drug, and to model a realistic worst-case scenario, we considered a single "synthetic" mutant defined as having the highest benefits (ρ, negative σ), lowest cost (s), and highest mutation rate of all the single-nucleotide mutants known for that drug. Each monotherapy simulation therefore tracked only two strains, wild type y_1 and mutant y_2. Simulations modeled 48-week trials, using discrete timesteps of $\Delta t = 30$ minutes. All simulations were done in Matlab R2010b. The following steps describe the simulation for a single patient on monotherapy, with expected adherence value α:

1. Draw from the viral load setpoint distribution in **Supplementary Figure 13a**. This setpoint is used to determine the value of the λ parameter, assuming that the patient has 3 L plasma.

    - In the suppression phase of therapy, the initial infection size is the setpoint, rounded to the nearest integer number of cells.

- In the maintenance phase of therapy, the initial infection size is the fully-suppressed infection size $\sum y_i \approx (\sum A_i)/d_y = 2$ c.ml^{-1}(RNA copies per ml).

2. Assign each infected cell to the mutant population (y_2) with probability u/s; otherwise the cell is in the wild-type population (y_1).

3. Identify all scheduled doses for the entire trial. All scheduled doses are evenly spaced, with the first dose occurring at the beginning of the trial. The patient takes each scheduled dose with probability α.

    - Exception: in the maintenance phase, the patient is always assumed to take the first scheduled dose.

4. Calculate the drug concentration every timestep, as described in Methods.

    - In the suppression phase, the initial drug concentration is zero.
    - In the maintenance phase, the initial drug concentration is C_{max}.

5. Calculate the basic reproductive ratios for the wild type and the mutant every timestep, as described in equations 1 and 2 of the main text and the Methods.

6. For each timestep:

    (a) The number of infected cells of strain i to exit the reservoir is drawn from a Poisson distribution with mean value $A_i \Delta t$.

    (b) The number of newly infected cells generated by strain i is drawn from a Poisson distribution with mean value $d_y y_i \Delta t \left[\frac{\lambda R_{0i}}{\lambda + \sum_{j=1}^{n} R_{0j} d_y y_j} \right]$.

    (c) Each cell newly infected by the wild type enters the mutant population with probability u; otherwise it remains wild type. Cells infected by the mutant do not back-mutate.

    (d) Each infected cell dies with probability $1 - \exp(-d_y \Delta t)$.

7. Determining outcome at 48 weeks:

    - In the suppression phase, the patient's status is observed at the end of the 48-week trial. If viral load is below 50 c.ml^{-1}, the trial is declared successful; otherwise virologic failure occurs.
    - In the maintenance phase, the patient's status is observed each week for 48 weeks, beginning at Week 5. If any two consecutive observations show a viral load of at least 200 c.ml^{-1}, virologic failure occurs; otherwise the trial succeeds.
    - A failed trial is considered a mutant-based failure if at least 20% of the viral population is mutant; otherwise it is considered a wild type-based failure.

8. Determining outcome over time:

    - Patient's status was evaluated every 2 weeks, for 48 weeks.
    - In the suppression phase, if viral load is below 50 c.ml^{-1} at the evaluation, the patient is classified as having "suppressed viral load;" otherwise the patient has "detectable viral load."
    - In the maintenance phase, the patient's viral load is measured each week for 48 weeks, beginning at Week 5. If any two consecutive measurements at or before the evaluation show a viral load of at least 200 c.ml^{-1}, the patient is declared to have "detectable viral load," and is then removed from the trial, retaining this classification for all future time-points. Otherwise, the patient is declared to have "suppressed viral load."
    - In the maintenance phase allowing recovery, the patient's viral load is measured as in the maintenance phase above. If viral load is at least 200 c.ml^{-1} both at the evaluation and at the immediately preceding measurement, the patient is declared to have "detectable viral load." Patients who were previously "detectable" remain in the trial and may re-suppress.

- A measurement of "detectable viral load" is considered "via resistance" if at least 20% of the viral population is mutant; otherwise it is considered to be "via wild type."

By using a well-mixed population and by assuming that the processes of reservoir exit, replication, and death are Poisson, this method implicitly sets the effective population size of the infection equal to the census size of infected cells. Population structure, selection on linked loci, and variations in burst size among infected cells are all mechanisms that could increase variance in viral offspring number, decreasing the effective population size[80;81]. Estimating the relevant population size to use for a model of drug resistance is difficult, as most approaches define an effective population size only for neutral loci. Simply "plugging in" a population size derived from a model without selection would be misleading in this context[82], and in lieu of a more informed value, we simply use the census size. This approach likely overestimates probabilities of mutant emergence and underestimates variability among patients[54; 83].

For dual therapy, we consider three strains: wild type, resistant to Drug 1, resistant to Drug 2. The two drugs can be simulated as two separate pills (allowing each pill to be taken or forgotten independently) or as a single combination pill (forcing the two drug concentrations to rise and fall in lockstep). In the case of two separate pills, the value of α may be different for each drug, allowing for "differential adherence" – which has been observed in some studies[35].

1.4 Graphing outcome versus adherence

For each monotherapy, 25,250 patients were simulated, with expected adherence α ranging from 0 to 1 (roughly equal numbers of patients were simulated for each 1% increment, including 50 patients with $\alpha = 0$ and 50 patients with $\alpha = 1$). The x-axis measures the *ex post* adherence for patients — that is, the actual percentage of doses taken, which may differ from the expectation α. Results were plotted for overlapping 2% windows, centered every 1% between 0 and 1, as well as

for the points 0 and 1 themselves.

Analysis of dual therapy with a combination pill was similar to that of monotherapy, but with 126,250 patients (including 250 patients with $\alpha = 0$ and 250 patients with $\alpha = 1$).

For dual therapy with separate pills, 169,000 patients were simulated, with expected adherences α_1, α_2 ranging from 0 to 1 (roughly equal numbers of patients were simulated for each 4% $\times$ 4% increment, including 25,000 patients on the border of the distribution where at least one α_i is equal to 0 or 1.) As with monotherapy, the axes measure *ex post* adherence. Results were plotted for overlapping 4% $\times$ 4% windows, centered every 2% between 0 and 1; points plotted on the border of the distribution show patients with at least one α_i exactly equal to 0 or 1.

Note that, for maintenance therapy, the axes do not include zero, as each patient is guaranteed to take the first dose (adherence is never zero).

1.5 Graphing outcome over time

Analysis was performed separately for each overlapping 2% adherence window, centered every 1% between 0 and 1, as well as for the points 0 and 1 themselves. The resulting graph shows a weighted average of these results, using the adherence distribution in **Supplementary Figure 13**. Measurements were taken every two weeks, and the graphs show the proportion of the population with each outcome. As there is no censoring of data, the analysis is equivalent to the Kaplan-Meier method[84].

1.6 MSW for combination therapy

For calculations involving combination therapy (limited to two drugs in this paper), viral fitness is influenced by the dose-response curves of all drugs. DRV and RAL belong to different classes and have been shown to reduce fitness in a multiplicative (Bliss-independent) fashion, which is often expected for drugs acting on different targets [27;28]. The equation describing viral fitness with two Bliss-independent drugs is given by:

$$R_0(D_1, D_2) = \frac{R_{00}}{\left(1 + \left(\frac{D_1}{IC_{50,1}}\right)^{m_1}\right)\left(1 + \left(\frac{D_2}{IC_{50,2}}\right)^{m_2}\right)} \tag{5}$$

where D_1, D_2 are the concentrations of each drug in the relevant compartment, $IC_{50,1}, IC_{50,2}$ are the concentrations at which 50% inhibition occurs, and m_1, m_2 are the slope parameters. The numerator R_{00} is the baseline basic reproductive ratio in the absence of drug treatment. Mutations that confer resistance to a given drug change the IC_{50}, slope and drug-free fitness similarly to the way described in equation 2 (main text).

For a two-drug combination where we assume that a viral strain may only be resistant to a single drug, there are now eight potential selection windows. Drug levels may be high enough for guaranteed treatment success; in the MSW for one or both drugs; in the overlapping region for one or both of the MSWs and the WGW, or strictly in the WGW. **Supplementary Figure 11** shows the possible windows for the RAL+DRV/r combination.

1.7 Derivation of Fig. 2f: comparing risk of wild type-based and mutant-based VF from selection window data

Figure 2f in the main text ranks drugs by the relative risk of mutant versus wild-type failure, regardless of the total risk of failure, based on the time spent in each selection window. The ranks are plotted along a line with values ranging from -1 (DRV/r and d4T, highest relative risk of wild-type failure) to 1 (FTC, the highest relative risk of mutant failure). This plot was constructed based on the data in **Figure 2a** in the main text. To devise this scale, we let

$$\begin{aligned} x &= \text{time until entry into MSW (days) / time until entry into WGW (days)} \\ &= \text{length of green bar / length of green + dark red bars,} \end{aligned} \tag{6}$$

$$\begin{aligned} y &= \text{time spent in MSW (days)} \\ &= \text{length of both red bars.} \end{aligned}$$

If the drug immediately enters the WGW at day 0, or if it skips the MSW completely, then x is defined to be 1.

Then the scale value to be plotted, a, is calculated as

$$a = \frac{y}{y_{max}} - x, \tag{7}$$

where $y_{max} \approx 16.5$ days, the maximum time that a drug spends in the MSW (obtained for FTC). Since both x and y/y_{max} range between 0 and 1, the scale ranges between -1 (failure via wild type only) and 1 (largest relative risk of resistance).

In this formula, x is a proxy for the rapidity of wild type-caused virologic failure ("wild-type

risk") relative to mutant-caused virologic failure ("mutant risk"). When x is small, the MSW window is reached long before the WGW, meaning that "mutant risk" is high and "wild-type risk" is low. When x is high, the WGW is reached soon after the MSW, or without ever entering the MSW, and so "wild-type risk" is high and "mutant risk" is low. While x considers how quickly the infection can start to grow, it does not consider the length of time in the MSW. Even if the MSW begins as soon as a dose is taken (so that $x = 0$), one still needs to consider for how long the mutant strain is selected over the wild-type to determine whether mutant-based or wild type-based virologic failure is more likely to occur. **Figure 12** shows a scatter plot of y versus x.

Supplementary Tables

Nature Medicine doi:10.1038/nm.2892

Table 1: Pharmacokinetic and pharmacodynamic parameters for anti-HIV drugs used in the study[17]

Class	Drug	IC_{50} (μMol)	slope	C_{max} (μMol)	half-life (hrs)	dosing (d^{-1})
NRTI	3TC	0.0298	1.15	15.3	10.0	2
	ABC	0.0381	0.93	10.5	21.0	2
	AZT	0.1823	0.85	4.5	8.5	2
	d4T	0.5524	1.13	2.3	3.5	2
	ddI	0.1795	1.07	39.4	18.0	1
	FTC	0.0079	1.20	7.3	39.0	1
	TDF	0.0561	0.97	1.1	60.0	1
NNRTI	EFV	0.0035	1.69	12.9	35.8	1
	ETV	0.0050	1.75	1.6	41	2
	NVP	0.0490	1.49	25.2	21.5	1
PI	ATV	0.0150	2.90	3.3	6.5	1
	ATV/r	0.0150	2.90	6.3	8.6	1
	DRV/r	0.0265	3.55	14.8	15.0	2
	IDV	0.0550	4.5	10.9	1.8	3
	IDV/r	0.0550	4.5	12.5	3.5	2
	LPV/r	0.0380	2.1	15.6	9.9	2
	NFV	0.2360	1.88	5.1	4.0	3
	SQV	0.0550	3.74	3.1	4.3	3
	SQV/r	0.0550	3.74	7.9	4.3	2
	TPV/r	0.2500	2.55	77.6	6.0	2
II	EVG	0.0280	0.94	1.7	8.6	1
	RAL	0.0150	1.03	4.0	10.0	2
FI	ENF	0.0349	1.60	1.1	3.8	2

Nature Medicine doi:10.1038/nm.2892

Table 2: Parameters for all single-point mutations considered in the study[17]

Class	Mutation	Cost (s)	u	Drug	ρ	σ
NRTI	K65R	0.41	1.1×10^{-5}	3TC	61	-0.19
				ABC	47	0.01
				ddI	20	-0.09
				FTC	29	-0.04
				TDF	43	0.00
	M184V	0.46	1.1×10^{-5}	3TC	963	-0.58
				ABC	9.5	-0.44
				AZT	0.28	-0.03
				ddI	9.5	-0.21
				FTC	1186	-0.49
				TDF	3.0	-0.27
	M41L	0.17	1.3×10^{-6}	AZT	2.2	0.07
				d4T	1.0	0.07
	T215Y	0.05	*	AZT	3.1	-0.34
				d4T	1.08	-0.12
NNRTI	G190S	0.79	2.2×10^{-5}	EFV	70	-0.40
				NVP	237	-0.34
	K101P	0.7	*	ETV	5.00	-0.27
	K103N	0.3	1.5×10^{-6}	EFV	85	-0.17
				NVP	94	-0.15
	Y181C	0.26	1.1×10^{-5}	EFV	2.6	-0.11
				ETV	11	-0.26
				NVP	234	-0.40
	Y181I	0.44	*	ETV	100	-0.37
				NVP	1309	-0.50

* Indicates mutation that requires two nucleotide changes;
mutation rate depends on prevalence of intermediate states.

Nature Medicine doi:10.1038/nm.2892

Table 3: Parameters for all single-point mutations considered in the study (Cont'd)[17]

Class	Mutation	Cost (s)	u	Drug	ρ	σ
PI	D30N	0.27	5.5×10^{-5}	NFV	2.3	-0.29
	G48V	0.45	8.5×10^{-7}	SQV	2.0	-0.23
	I47A	0.9	*	LPV	5.8	-0.40
	I47V	0.05	1.1×10^{-5}	LPV	1.8	-0.29
	I50L	0.75	9.0×10^{-7}	ATV	1.2	-0.34
	I50V	0.93	1.1×10^{-5}	DRV	0.68	-0.07
	I54L	0.05	9.0×10^{-7}	DRV	0.98	-0.01
	I84V	0.82	1.1×10^{-5}	ATV	0.60	-0.34
				DRV	0.94	-0.01
				IDV	0.73	-0.39
				TPV	0.26	-0.39
	L33F	0.49	6.3×10^{-6}	TPV	1.4	0.02
	L90M	0.30	3.2×10^{-6}	NFV	1.5	0.01
				SQV	1.1	-0.28
	M46I	0.05	5.6×10^{-5}	IDV	1.0	-0.29
	M46L	0.05	1.3×10^{-6}	IDV	0.76	-0.24
	N88S	0.55	1.1×10^{-5}	ATV	3.1	-0.31
	V32I	0.09	4.1×10^{-5}	LPV	0.53	-0.16
	V82A	0.59	1.1×10^{-5}	LPV	1.03	-0.33
	V82F	0.79	3.4×10^{-7}	IDV	0.89	-0.58
				LPV	1.45	-0.44
	V82T	0.22	*	IDV	0.98	-0.34
				LPV	0.87	-0.17
				TPV	0.68	-0.20
II	G140S	0.71	2.2×10^{-5}	RAL	2.1	0.03
	N155H	0.55	5.3×10^{-7}	EVG	20	0.00
				RAL	27	0.02
	Q148H	0.73	2.0×10^{-6}	EVG	6.8	-0.04
				RAL	86	0.06
	Q148K	0.76	6.5×10^{-6}	EVG	19	0.03
				RAL	128	-0.06
	Q148R	0.61	1.1×10^{-5}	EVG	68	0.06
				RAL	90	0.04
	Y143C	0.74	1.1×10^{-5}	RAL	3.6	0.06
	Y143H	0.55	1.1×10^{-5}	RAL	2.7	-0.04
	Y143R	0.32	*	RAL	75	-0.01
FI	G36D	0.12	2.2×10^{-5}	ENF	1.7	-0.45
	N42T	0.54	5.3×10^{-7}	ENF	2.9	-0.13
	N43D	0.88	1.1×10^{-5}	ENF	13	-0.06
	Q40H	0.26	1.5×10^{-6}	ENF	12	-0.31
	V38A	0.17	1.1×10^{-5}	ENF	11	-0.32

* Indicates mutation that requires two nucleotide changes; mutation rate depends on prevalence of intermediate states.

Nature Medicine doi:10.1038/nm.2892

Table 4: Parameters for pre-existing frequency of mutations and exit rate from the latent reservoir. See **Methods** and **Supplemental Methods** for explanations.

class	mutation	equilibrium frequency	reservoir exit (days)
NRTI	K65R	2.7×10^{-5}	12
	M184V	2.4×10^{-5}	14
	M41L	7.8×10^{-6}	43
	T215Y	*	*
NNRTI	G190S	2.8×10^{-5}	12
	K101P	*	*
	K103N	4.9×10^{-6}	68
	Y181C	4.3×10^{-5}	8
	Y181I	*	*
PI	D30N	2.0×10^{-4}	2
	G48V	1.9×10^{-6}	177
	I47A	*	*
	I47V	2.2×10^{-4}	2
	I50L	1.2×10^{-6}	279
	I50V	1.2×10^{-5}	28
	I54L	1.8×10^{-5}	19
	I84V	1.4×10^{-5}	25
	L33F	1.3×10^{-5}	26
	L90M	1.1×10^{-5}	31
	M46I	1.1×10^{-3}	< 0.5
	M46L	2.6×10^{-5}	13
	N88S	2.0×10^{-5}	17
	V32I	4.6×10^{-4}	1
	V82A	1.9×10^{-5}	18
	V82F	4.3×10^{-7}	769
	V82T	*	*
II	G140S	3.1×10^{-5}	11
	N155H	9.6×10^{-7}	349
	Q148H	2.0×10^{-6}	166
	Q148K	8.5×10^{-6}	39
	Q148R	1.8×10^{-5}	18
	Y143C	1.5×10^{-5}	22
	Y143H	2.0×10^{-5}	17
	Y143R	*	*
FI	G36D	1.8×10^{-4}	2
	N42T	9.8×10^{-7}	342
	N43D	1.3×10^{-5}	27
	Q40H	5.6×10^{-6}	59
	V38A	6.5×10^{-5}	5

* Indicates mutation that requires two nucleotide changes;
equilibrium frequency depends on prevalence of intermediate states.

Nature Medicine doi:10.1038/nm.2892

Table 5: Parameters for pre-existing frequency and exit rate from the latent reservoir for best "synthetic" mutation for each drug. See Methods and Supplemental Methods for explanations.

class	drug	equilibrium frequency	reservoir exit (days)
NRTI	AZT	2.4×10^{-5}	14
	d4T	7.8×10^{-6}	43
	3TC	2.7×10^{-5}	12
	FTC	2.7×10^{-5}	12
	ABC	2.7×10^{-5}	12
	ddI	2.7×10^{-5}	12
	TDF	2.7×10^{-5}	12
NNRTI	EFV	4.3×10^{-5}	8
	NVP	4.3×10^{-5}	8
	ETV	4.3×10^{-5}	8
PI	DRV	1.8×10^{-5}	19
	NFV	2.0×10^{-4}	2
	SQV	1.1×10^{-5}	31
	LPV	4.6×10^{-4}	1
	ATV	2.0×10^{-5}	17
	IDV	1.1×10^{-3}	< 0.5
	TPV	1.4×10^{-5}	25
II	RAL	3.1×10^{-5}	11
	EVG	1.8×10^{-5}	18
FI	ENF	1.8×10^{-4}	2

Table 6: Viral dynamics parameters in the absence of drug therapy

	Parameter	Value	Units	Reference
R_{00}	Baseline basic reproduction ratio	10	(unitless)	See text
d_y	Death rate of actively infected cells	1	d^{-1}	[66]
v_0	Residual plasma viral load maintained by activation from latent reservoir, absent viral replication	2	RNA copies per ml plasma	[73]
A	Latent reservoir exit rate	3000	cells.d^{-1}	Based on v_0, see text

Nature Medicine doi:10.1038/nm.2892

Table 7: Nucleotide substitution rate parameters for HIV. Each entry gives the per-site transition probability from row base to column base in one round of viral replication. For derivation and source see Section 1.2.4. The extraordinary skew of this matrix (the largest entry, G-to-A mutation, is more than 300 times the smallest, C-to-G mutation) reflects the base composition of the genome, particularly the bias towards A. Values less than 10^{-6} are particularly uncertain, as they were computed from fewer than 5 substitution observations each.

	U	C	A	G
U		1.1×10^{-5}	1.3×10^{-5}	3.6×10^{-6}
C	2.4×10^{-5}		6.5×10^{-6}	1.7×10^{-7}
A	7.9×10^{-7}	5.3×10^{-7}		1.1×10^{-5}
G	8.5×10^{-7}	8.5×10^{-7}	5.5×10^{-5}	

Supplementary Figures

Nature Medicine doi:10.1038/nm.2892

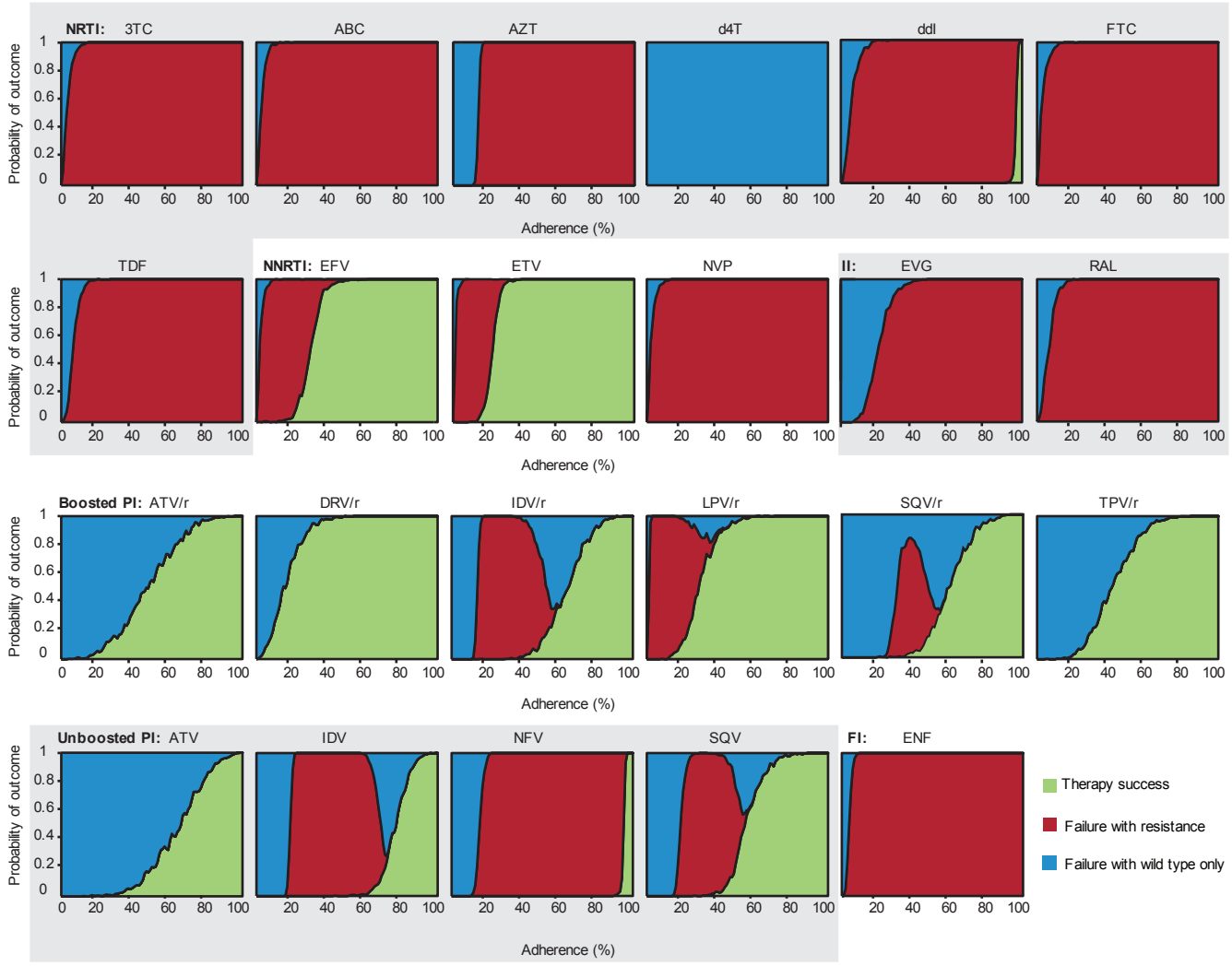

Figure 1: Simulated clinical outcomes versus adherence for all drugs. In "Suppression" trials, patients begin with a realistic distribution of treatment-naive viral loads (between 3000 and 10^6 c.ml^{-1}) and undergo monotherapy for a full 48 weeks. Virologic failure (VF) is defined as a viral load above 50 c.ml^{-1}at Week 48. VF is classified as "via resistance" if at least 20% of the viral population at the time of detection is mutant. Adherence (x-axis) is measured as the fraction of scheduled doses taken. The height of the area shaded indicates probability of the corresponding outcome at that adherence level. 3TC, lamivudine; ABC, abacavir; AZT, zidovudine; d4T, stavudine; ddI, didanosine, FTC, emtricitabine; TDF, tenofovir disoproxil fumarate; EFV, efavirenz; ETV, etravirine; NVP, nevirapine; ATV, atazanavir; DRV, darunavir; IDV, indinavir; LPV, lopinavir; NFV, nelfinavir; SQV, saquinavir; TPV, tipranavir; EVG, elvitegravir; RAL, raltegravir; ENF, enfuvirtide.

Nature Medicine doi:10.1038/nm.2892

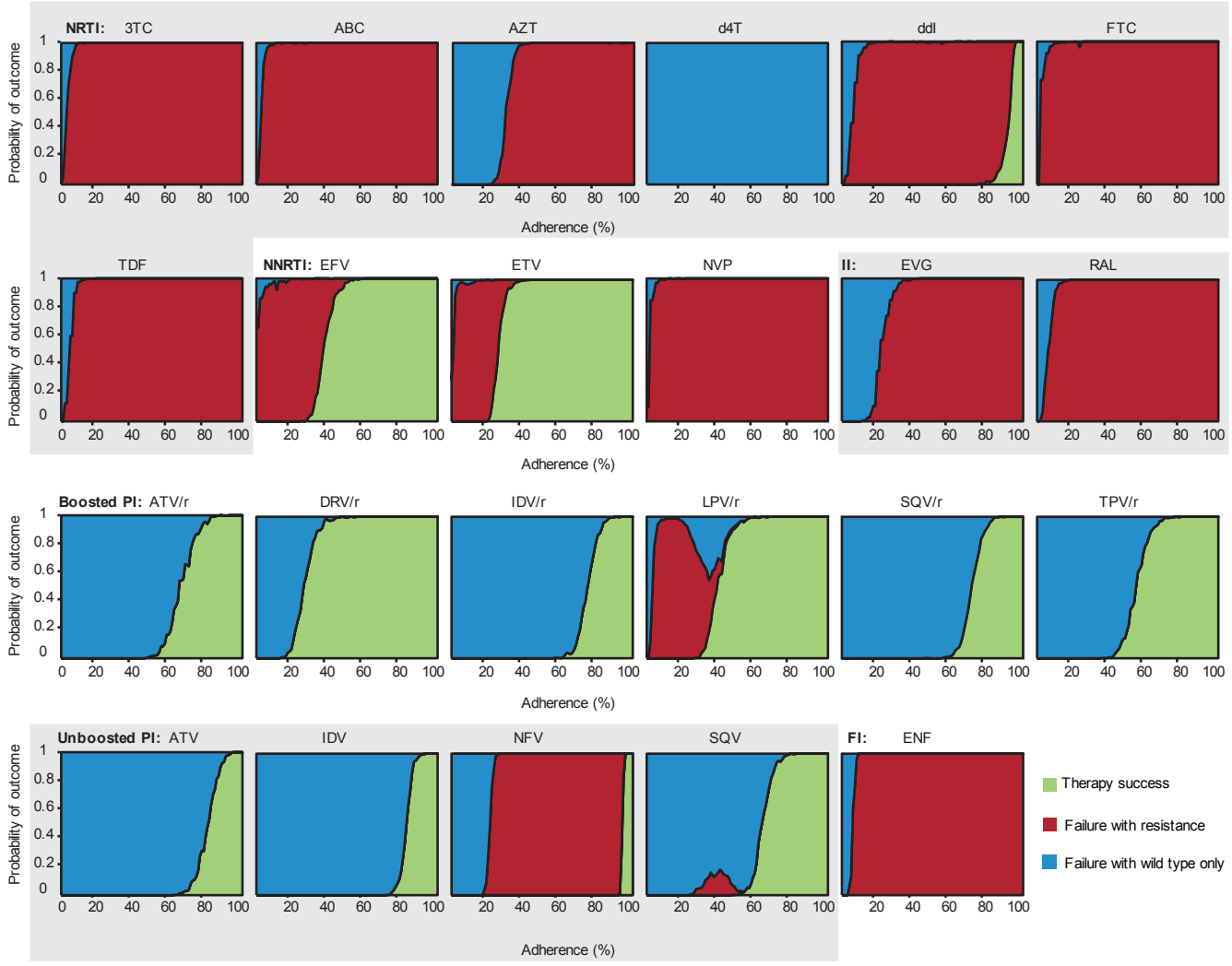

Figure 2: Simulated clinical outcomes versus adherence for all drugs. In "Maintenance" trials, patients begin with full viral suppression and undergo monotherapy for 48 weeks or until virologic failure (VF), whichever occurs first. VF is defined as "confirmed rebound": two consecutive weekly measurements (starting at week 5) with viral load above 200 c.ml^{-1}. VF is classified as "via resistance" if at least 20% of the viral population at the time of detection is mutant. Adherence (x-axis) is measured as the fraction of scheduled doses taken. The height of the area shaded indicates probability of the corresponding outcome at that adherence level.

Nature Medicine doi:10.1038/nm.2892

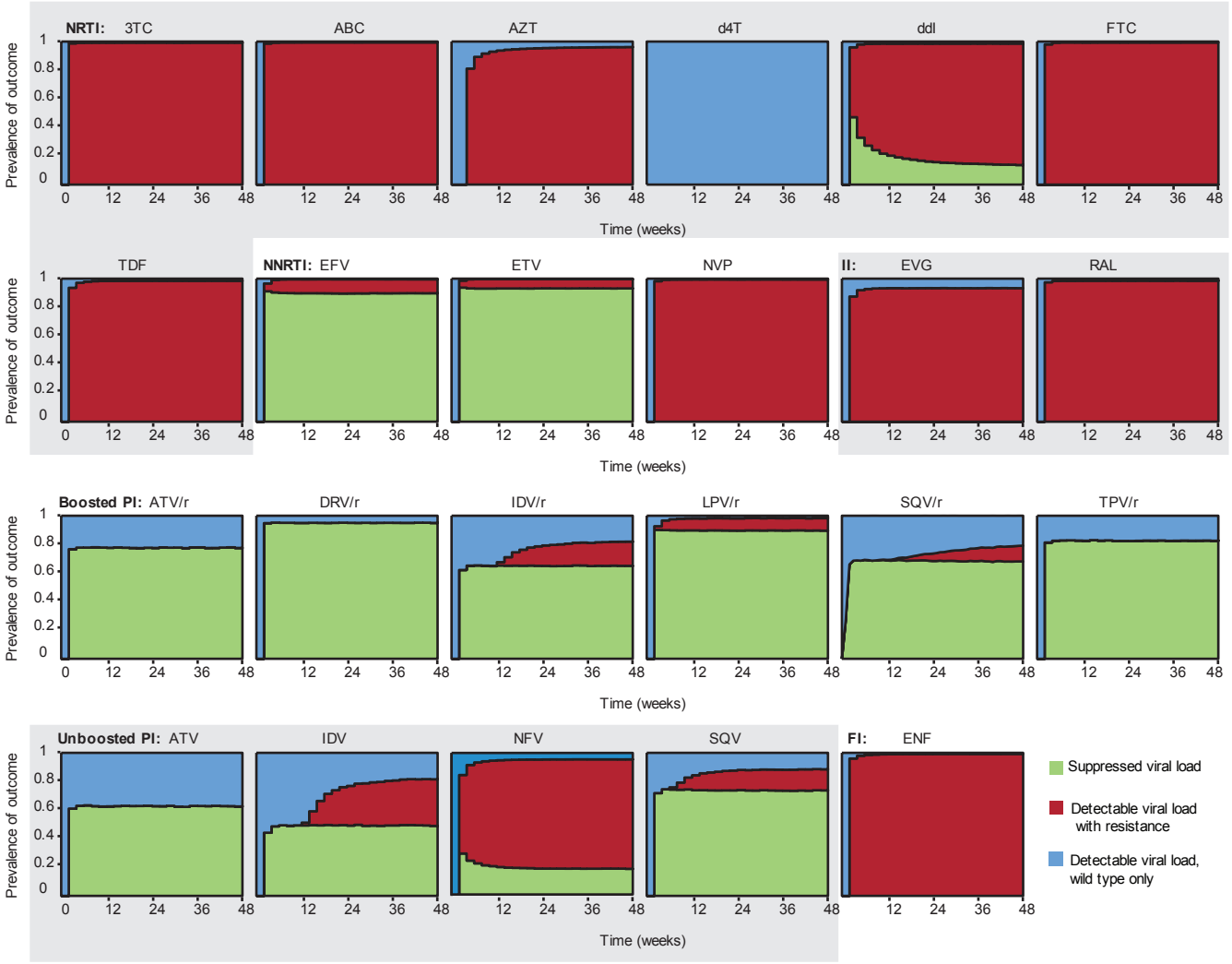

Figure 3: Simulated clinical outcomes versus time for all drugs. In "Suppression" trials, patients begin with a realistic distribution of treatment-naive viral loads (between 3000 and 10^6 c.ml^{-1}) and undergo monotherapy for a variable time (x-axis). "Detectable viral load" is defined as above 50 c.ml^{-1}and is classified as "via resistance" if at least 20% of the viral population at the time of detection is mutant. The height of the area shaded indicates prevalence of the corresponding outcome at that time. Patients have a realistic distribution of adherence levels with an average of 70%.

Nature Medicine doi:10.1038/nm.2892

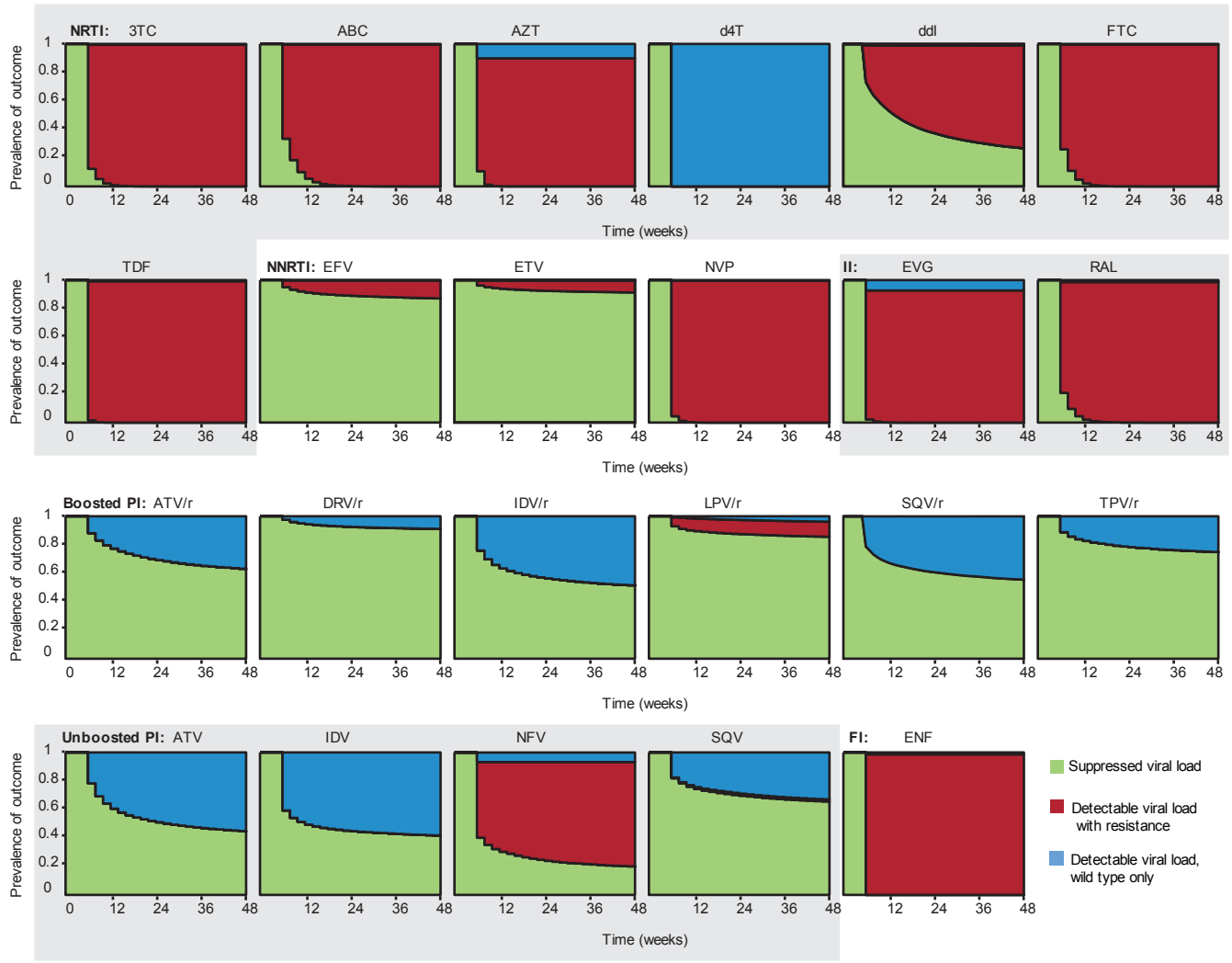

Figure 4: Simulated clinical outcomes versus time for all drugs. In "Maintenance" trials, patients begin the trial with full viral suppression and undergo monotherapy for a variable amount of time (x-axis) or until "detectable viral load" is observed, whichever occurs first. "Detectable viral load" is defined as "confirmed rebound": two consecutive weekly measurements (starting at Week 5) above 200 c.ml^{-1}. It is classified as "via resistance" if at least 20% of the viral population at the time of detection is mutant. The height of the area shaded indicates prevalence of the corresponding outcome at that time. Patients have a realistic distribution of adherence levels with an average of 70%.

Nature Medicine doi:10.1038/nm.2892

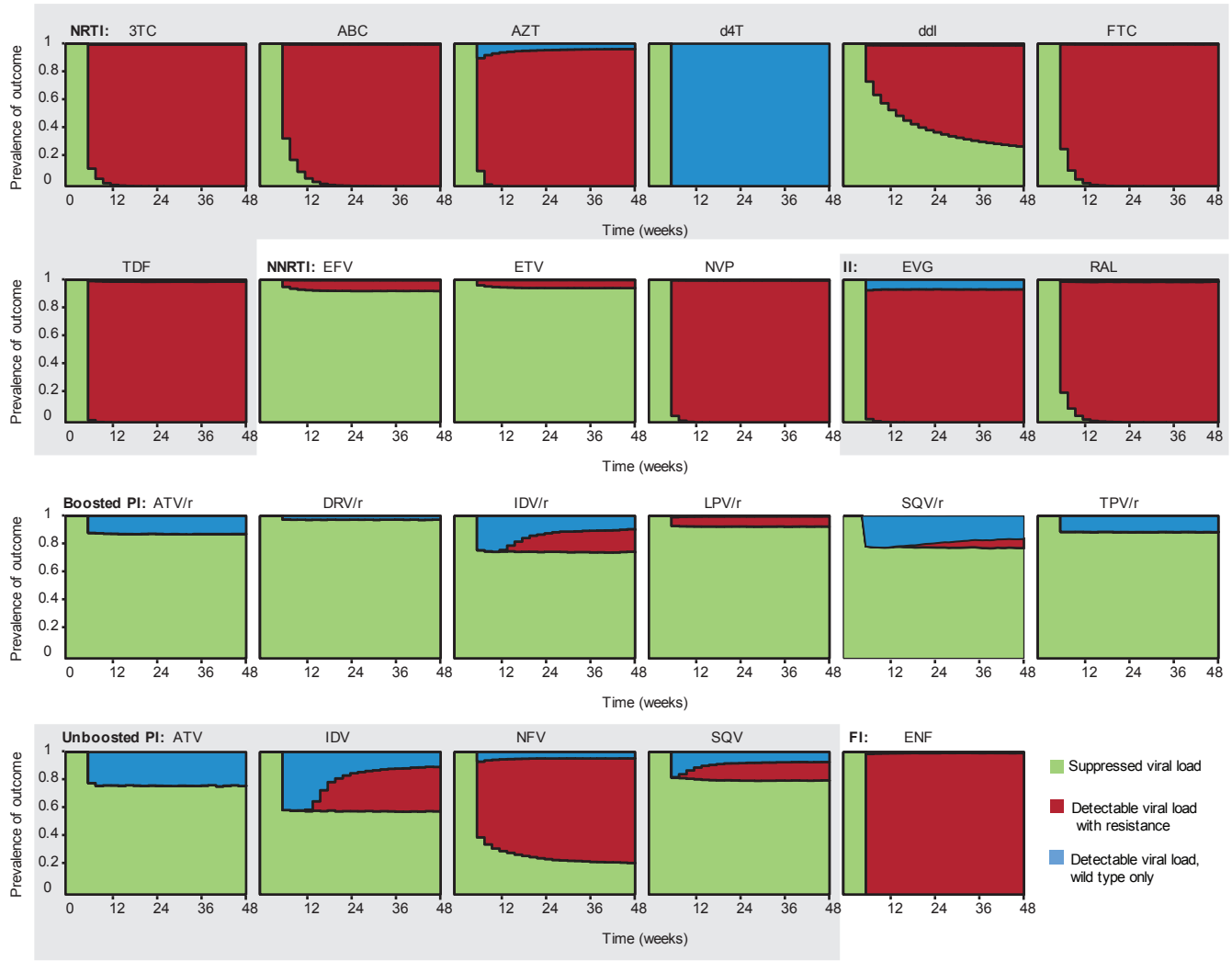

Figure 5: Simulated clinical outcomes versus time for all drugs. In "Maintenance with recovery" trials, patients begin the trial with full viral suppression and undergo monotherapy for a variable amount of time (x-axis). "Detectable viral load" is defined as "confirmed rebound": two consecutive weekly measurements (starting at Week 5) with viral load above 200 c.ml^{-1}. It is classified as "via resistance" if at least 20% of the viral population at the time of detection is mutant. We allow recovery, meaning that patients stay in the trial to see if they will re-suppress, instead of being removed immediately like in regular "Maintenance" trials. The height of the area shaded indicates prevalence of the corresponding outcome at that time-point. Patients have a realistic distribution of adherence levels with an average of 70%.

Nature Medicine doi:10.1038/nm.2892

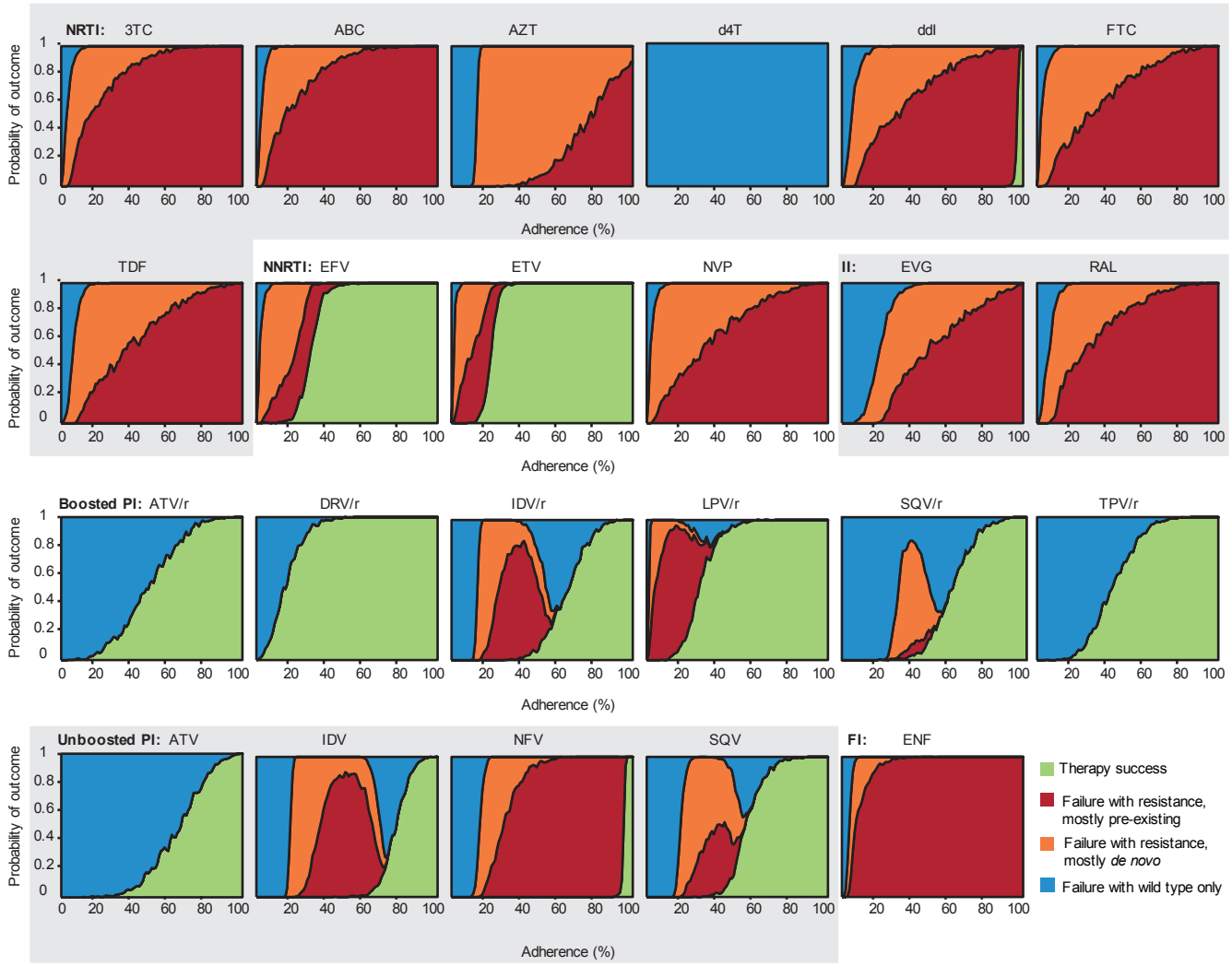

Figure 6: Simulated clinical outcomes versus adherence for all drugs, distinguishing pre-existing from *de novo* mutations. In the "Suppression" trials shown, patients begin with a realistic distribution of treatment-naive viral loads (between 3000 and 10^6 c.ml^{-1}) and undergo monotherapy for a full 48 weeks. Virologic failure (VF) is defined as a viral load above 50 c.ml^{-1}at Week 48. VF is classified as "via resistance" if at least 20% of the viral population at the time of detection is mutant. Resistance is classified as *de novo* if the majority of mutants at the time of failure descended from a mutation event that occurred during replication since the start of the trial. Otherwise, resistance is classified as "pre-existing," which includes mutants arising from both the pre-treatment plasma population and the latent reservoir. Adherence (x-axis) is measured as the fraction of scheduled doses taken. The height of the area shaded indicates probability of the corresponding outcome at that adherence level.

Nature Medicine doi:10.1038/nm.2892

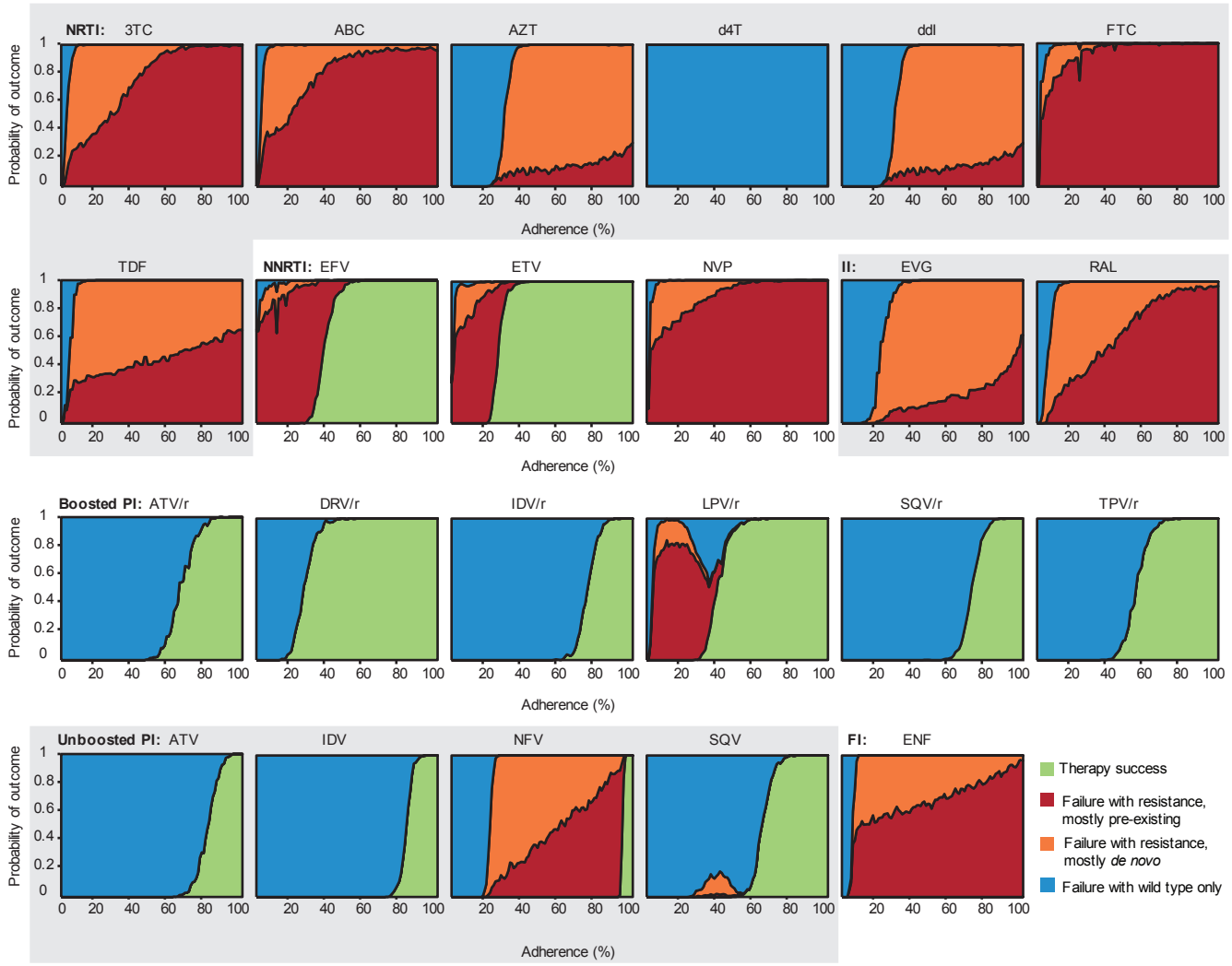

Figure 7: Simulated clinical outcomes versus adherence for all drugs, distinguishing pre-existing from *de novo* mutations. In the "Maintenance" trials shown, patients begin with full viral suppression and undergo monotherapy for 48 weeks or until virologic failure (VF), whichever occurs first. VF is defined as "confirmed rebound": two consecutive weekly measurements (starting at Week 5) with viral load above 200 c.ml^{-1}. VF is classified as "via resistance" if at least 20% of the viral population at the time of detection is mutant. Resistance is classified as *de novo* if the majority of mutants at the time of failure descended from a mutation event that occurred during replication since the start of the trial. Otherwise, resistance is classified as "pre-existing," which includes mutants arising from both the pre-treatment plasma population and the latent reservoir. Adherence (x-axis) is measured as the fraction of scheduled doses taken. The height of the area shaded indicates probability of the corresponding outcome at that adherence level.

Nature Medicine doi:10.1038/nm.2892

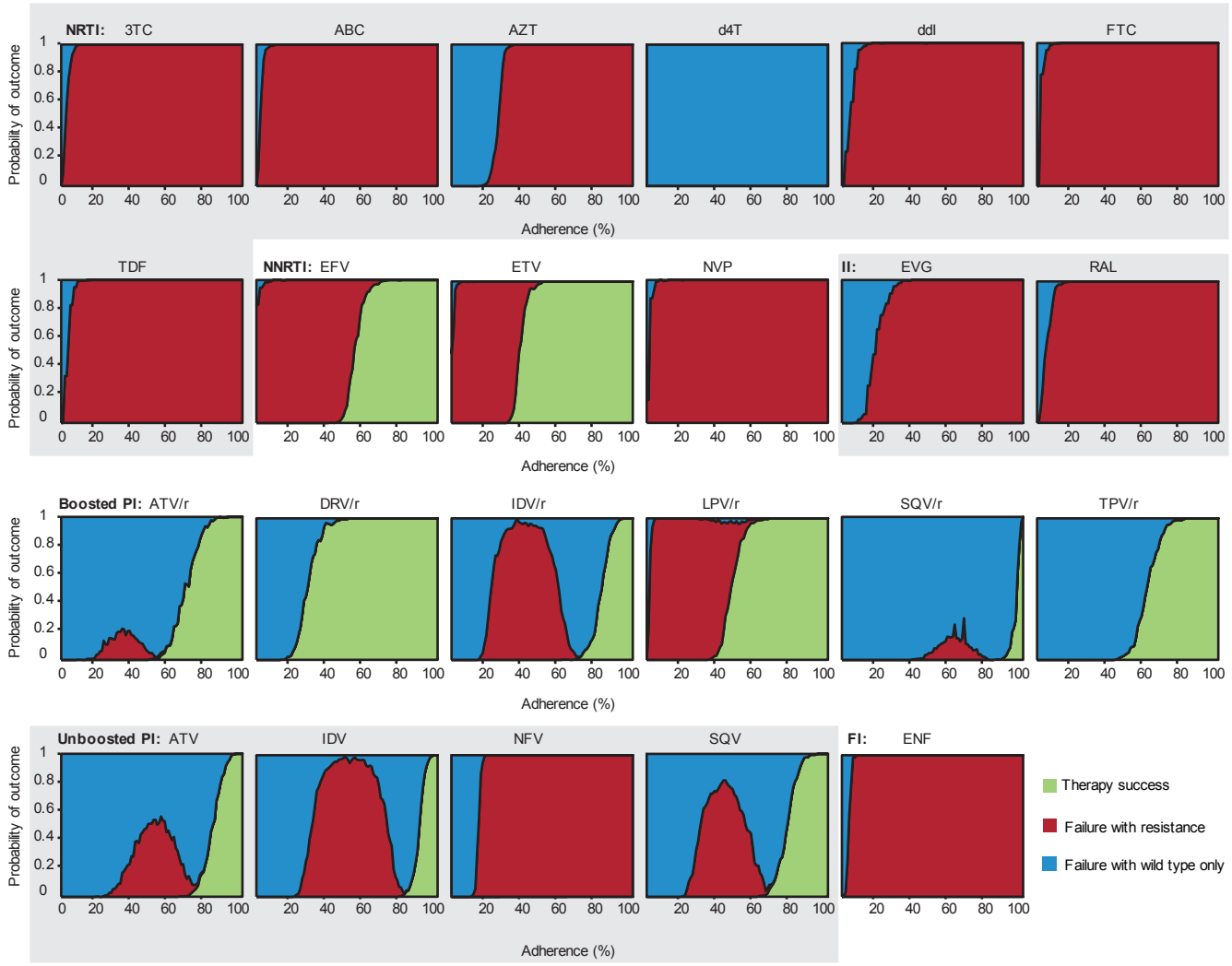

Figure 8: Simulated clinical outcomes versus adherence for all drugs, R_{00}=20. Results are shown for "Maintenance" trials only. In the "Maintenance" trials shown, patients begin with full viral suppression and undergo monotherapy for 48 weeks or until virologic failure (VF), whichever occurs first. VF is defined as "confirmed rebound": two consecutive weekly measurements (starting at Week 5) with viral load above 200 c.ml^{-1}. VF is classified as "via resistance" if at least 20% of the viral population at the time of detection is mutant. Adherence (x-axis) is measured as the fraction of scheduled doses taken. The height of the area shaded indicates probability of the corresponding outcome at that adherence level. As compared to R_{00}=10, increasing R_{00} to 20 leads to higher adherence levels being required for treatment success, and it extends the range of adherence levels (in both directions) for which resistant strains can cause failure. Mutant VF becomes a possible outcome for the PIs ATV, ATV/r, IDV, IDV/r, and SQV/r, and treatment success cannot occur at any adherence level for ddI and NFV.

Nature Medicine doi:10.1038/nm.2892

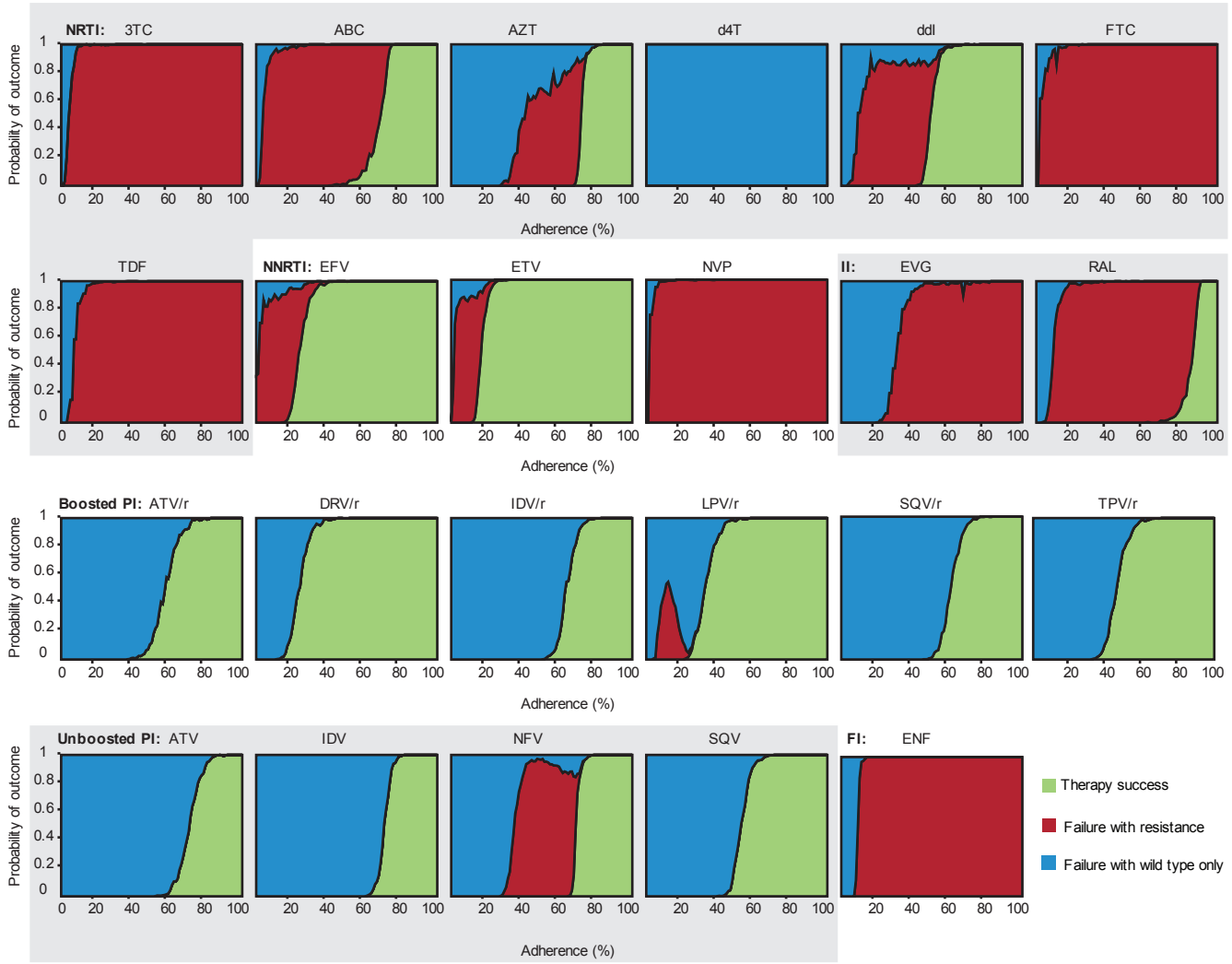

Figure 9: Simulated clinical outcomes versus adherence for all drugs, R_{00}=5. Results are shown for "Maintenance" trials only. In the "Maintenance" trials shown, patients begin with full viral suppression and undergo monotherapy for 48 weeks or until virologic failure (VF), whichever occurs first. VF is defined as "confirmed rebound": two consecutive weekly measurements (starting at Week 5) with viral load above 200 c.ml^{-1}. VF is classified as "via resistance" if at least 20% of the viral population at the time of detection is mutant. Adherence (x-axis) is measured as the fraction of scheduled doses taken. The height of the area shaded indicates probability of the corresponding outcome at that adherence level. As compared to R_{00}=10, decreasing R_{00} to 5 leads to lower adherence levels being required for treatment success, and it reduces the range of adherence levels for which resistant strains can cause failure. A range of high adherence levels appears where there is treatment success for ABC and AZT, and near-perfect adherence is no longer required for ddI and NFV success. Mutant VF no longer occurs for SQV, and for AZT and ddI, wild-type failure may be the first outcome to occur as adherence levels decrease from the successful range.

Nature Medicine doi:10.1038/nm.2892

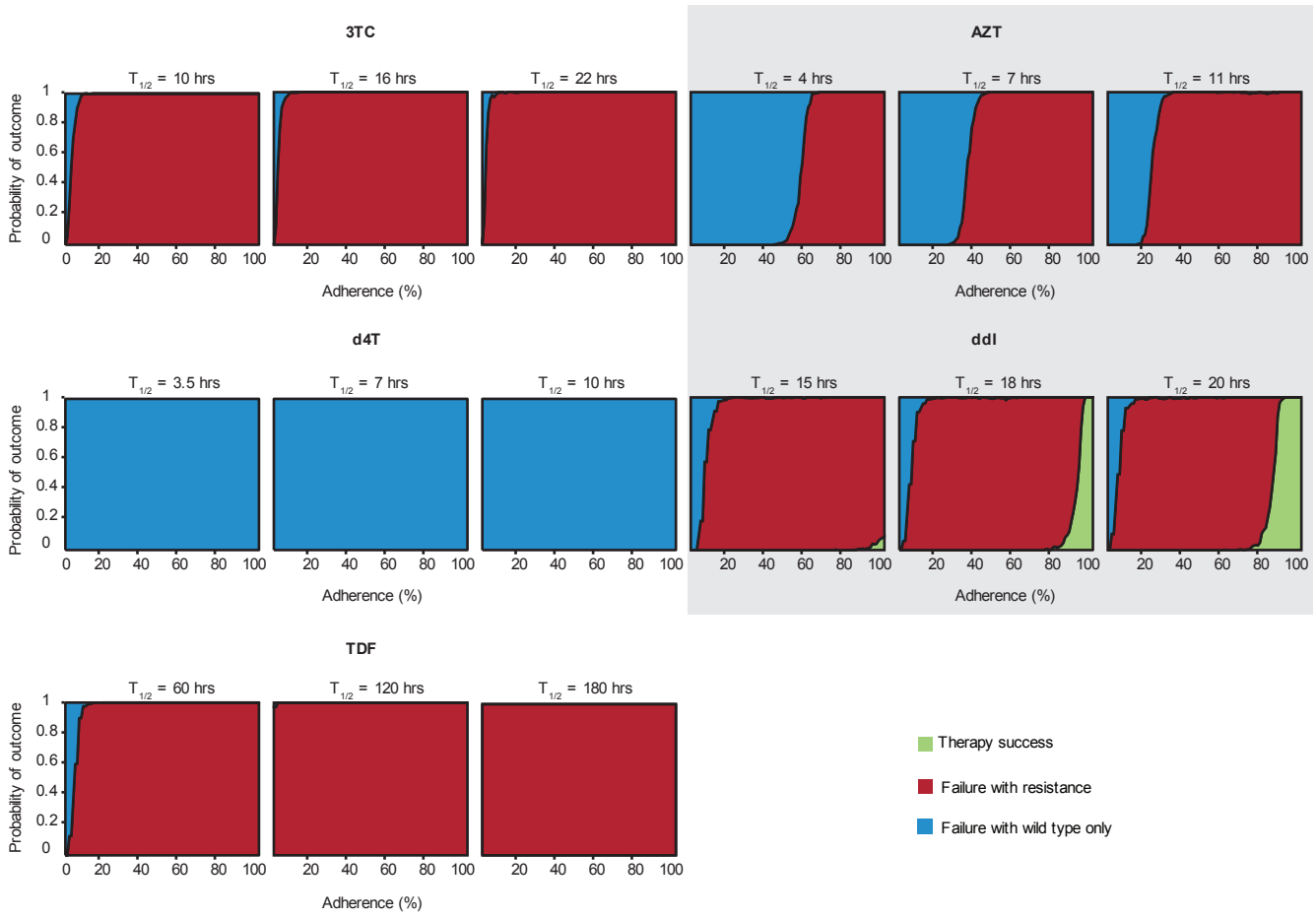

Figure 10: Simulated clinical outcomes versus adherence for NRTIs with large inter-experimental variation in half-life. The ranges included were {10, 16, 22} for 3TC, {4, 8.5, 11} for AZT, {3.5, 7, 10} for d4T, {15, 18, 20} for ddI, and {60, 120, 180} for TDF. Results are shown for "Maintenance" trials only. In the "Maintenance" trials shown, patients begin with full viral suppression and undergo monotherapy for 48 weeks or until virologic failure (VF), whichever occurs first. VF is defined as "confirmed rebound": two consecutive weekly measurements (starting at Week 5) with viral load above 200 c.ml^{-1}. VF is classified as "via resistance" if at least 20% of the viral population at the time of detection is mutant. Adherence (x-axis) is measured as the fraction of scheduled doses taken. The height of the area shaded indicates probability of the corresponding outcome at that adherence level. Compared to the half-lives used throughout the rest of the paper (see **Supplementary Table 1**), the results barely change for 3TC or d4T. For AZT, varying the half-life changes the adherence level where wild-type failure becomes more likely than mutant failure. For ddI, the adherence level where treatment success occurs shifts. For higher TDF half-lives, mutant VF becomes the only outcome, with the exception of rare (< 3%) wild-type failure at the lowest adherence levels for $t_{1/2} = 120$ hours.

Nature Medicine doi:10.1038/nm.2892

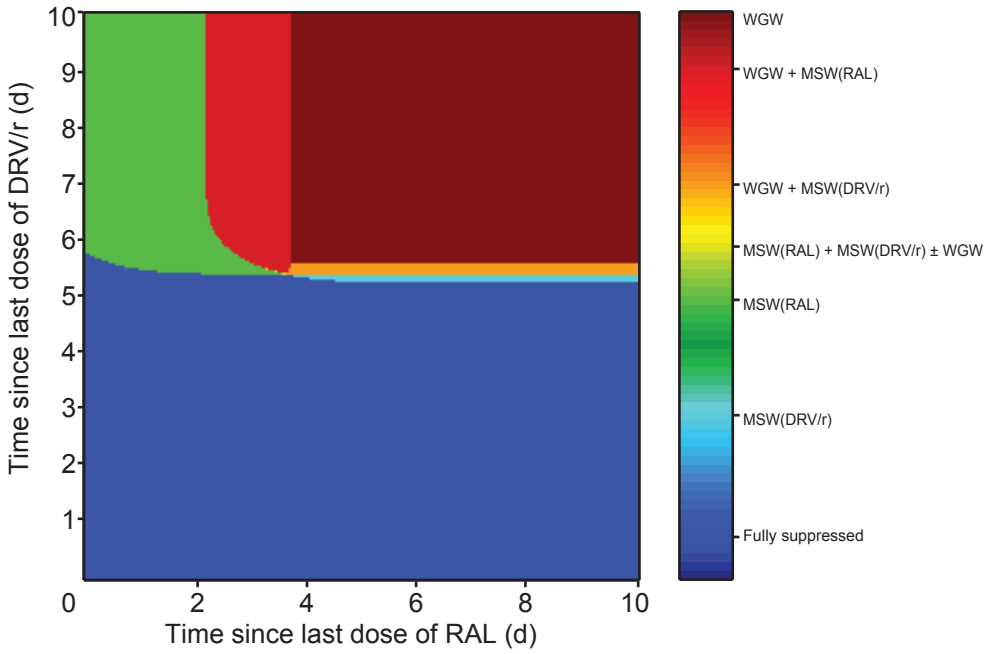

Figure 11: Selection regimes for DRV/r-RAL two-drug therapy. Depending on the length of a treatment interruption to one or both drugs, treatment may be fully suppressive or select for the wild-type strain, a mutant resistant to DRV, a mutant resistant to RAL, or combinations of these strains. The yellow region, where the MSW for both drugs overlap, is barely visible, and it is located where the other MSW regions meet, near the center of the graph.

Nature Medicine doi:10.1038/nm.2892

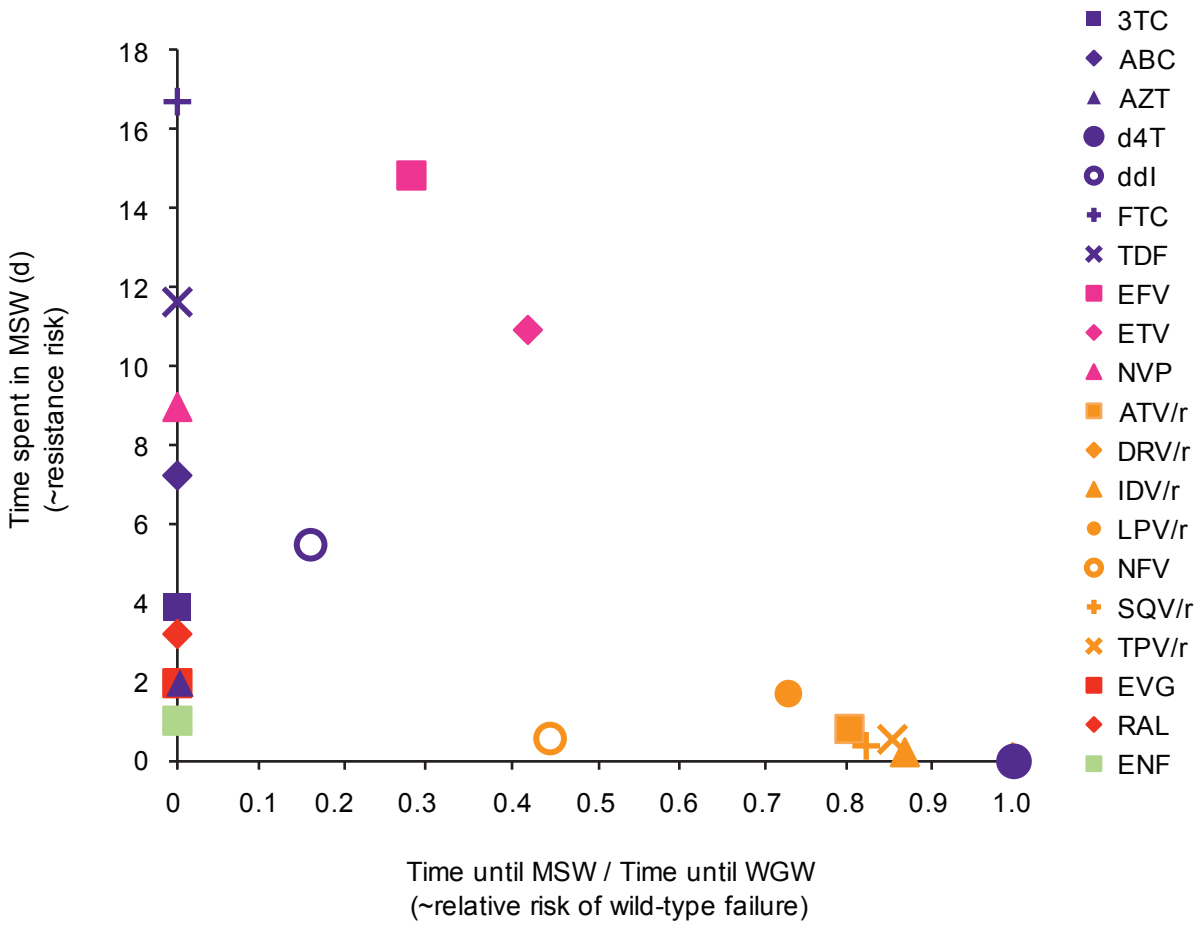

Figure 12: Relative risk of wild type- vs. mutant-caused virologic failure for anti-HIV drugs, considering the best "synthetic" mutation defined in Section 1.3. Two metrics can be used to compare the risk of resistance to the likelihood of wild-type growth, shown on both axes. The x-axis measures the time until a patient interrupting treatment reaches the MSW, divided by the time until that patient reaches the WGW. The y-axis measures the number of days that a patient spends in the MSW during a treatment interruption. Drugs tend to cluster near the endpoints of the x-axis: most NRTIs, the IIs, and the FI are on the left, meaning that the patient enters the MSW immediately or soon after interruption, and most PIs are on the right, meaning that the patient waits relatively long to enter the MSW. Section 1.7 further describes the two metrics and explains how they were used in **Figure 2f** in the main text to rank the drugs by relative risk of mutant-based versus wild type-based VF. Note that the symbol for DRV/r is obscured behind the symbol for d4T at $(1, 0)$.

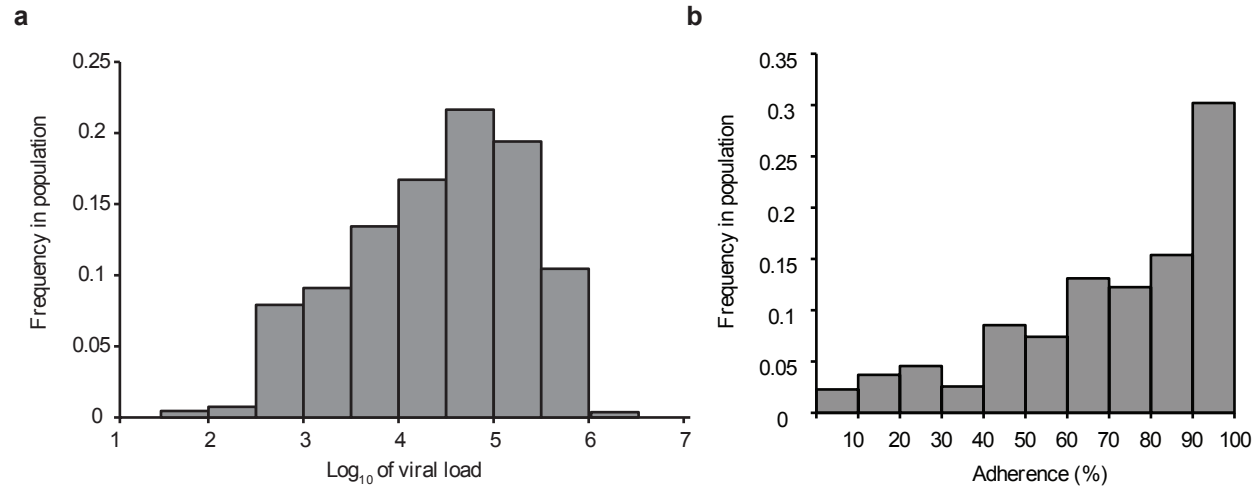

Figure 13: Distribution of a) viral load setpoints[85] (data available at www.hiv.lanl.gov/content/immunology) and b) adherence levels[30] used in simulations.

References

[66] Markowitz, M., *et al.* A novel antiviral intervention results in more accurate assessment of human immunodeficiency virus type 1 replication dynamics and T-Cell decay in vivo. *J. Virol.* **77**(8), 5037–5038 (2003).

[67] Little, S. J., McLean, A. R., Spina, C. A., Richman, D. D., & Havlir, D. V. Viral dynamics of acute HIV-1 infection. *J. Exp. Med.* **190**(6), 841 –850 (1999).

[68] Davey, Jr., R. T., *et al.* HIV-1 and T cell dynamics after interruption of highly active antiretroviral therapy (haart) in patients with a history of sustained viral suppression. *Proc. Natl. Acad. Sci. USA* **96**(26), 15109–15114 (1999).

[69] Ioannidis, J. P. A., *et al.* Dynamics of HIV-1 viral load rebound among patients with previous suppression of viral replication. *AIDS* **14**, 1481–1488 (2000).

[70] Krakovska, O. & Wahl, L. M. Costs versus benefits: best possible and best practical treatment regimens for HIV. *J. Math. Biol.* **54**, 385–406 (2007).

[71] Funk, G. A., *et al.* Quantification of in vivo replicative capacity of HIV-1 in different compartments of infected cells. *J. Acquir. Immune Defic. Syndr.* **26**(5), 397–404 (2001).

[72] Putter, H., Heisterkamp, S. H., Lange, J. M. A., & de Wolf, F. A Bayesian approach to parameter estimation in HIV dynamical models. *Statist. Med.* **21**(15), 2199–2214 (2002).

[73] Dinoso, J. B., *et al.* Treatment intensification does not reduce residual HIV-1 viremia in patients on highly active antiretroviral therapy. *Proc. Natl. Acad. Sci. USA* **106**(23), 9403 (2009).

[74] Hockett, R. D., *et al.* Constant mean viral copy number per infected cell in tissues regardless of high, low, or undetectable plasma HIV RNA. *J. Exp. Med.* **189**(10), 1545 –1554 (1999).

[75] De Boer, R. J., Ribeiro, R. M., & Perelson, A. S. Current estimates for HIV-1 production imply rapid viral clearance in lymphoid tissues. *PLoS Comput. Biol.* **6**(9), e1000906 (2010).

[76] Sedaghat, A., Siliciano, R. F., & Wilke, C. O. Low-level HIV-1 replication and the dynamics of the resting CD4+ t cell reservoir for HIV-1 in the setting of HAART. *BMC Inf. Dis.* **8**(1), 2 (2008).

[77] Mansky, L. M. & Temin, H. M. Lower in vivo mutation rate of human immunodeficiency virus type 1 than that predicted from the fidelity of purified reverse transcriptase. *J. Virol.* **69**(8), 5087–5094 (1995).

[78] Abram, M. E., Ferris, A. L., Shao, W., Alvord, W. G., & Hughes, S. H. Nature, position, and frequency of mutations made in a single cycle of HIV-1 replication. *J. Virol.* **84**, 9864–9878, October (2010).

[79] Kuiken, C., *et al.*, editors. *HIV Sequence Compendium 2010*. Theoretical Biology and Biophysics Group, Los Alamos National Laboratory, NM, (2010).

[80] Achaz, G., *et al.* A robust measure of HIV-1 population turnover within chronically infected individuals. *Mol. Biol. Evol.* **21**(10), 1902–1912 (2004).

[81] Frost, S. D., Nijhuis, M., Schuurman, R., Boucher, C. A., & Leigh Brown, A. J. Evolution of lamivudine resistance in human immunodeficiency virus type 1-infected individuals: the relative roles of drift and selection. *J. Virol.* **74**(14), 6262–6268 (2000).

[82] Kouyos, R. D., Althaus, C. L., & Bonhoeffer, S. Stochastic or deterministic: what is the effective population size of HIV-1? *Trends Microbiol.* **14**(12), 507–511 (2006).

[83] Pennings, P. S. Standing genetic variation and the evolution of drug resistance in HIV. *PLoS Comput Biol* **8**(6), e1002527, June (2012).

[84] Kaplan, E. L. & Meier, P. Nonparametric estimation from incomplete observations. *J. Amer. Statist. Assoc.* **53**(282), 457–481 (1958).

[85] Kiepiela, P., *et al.* Dominant influence of HLA-B in mediating the potential co-evolution of HIV and HLA. *Nature* **432**(7018), 769775 (2004).